Extreme-value forest fire prediction: A study of the Loss Function in an Ordinality Scheme

Nicolas Caron* Hassan Noura† Christophe Guyeux‡ Benjamin Aynes§

Abstract

Wildfires are highly imbalanced natural hazards in both space and severity, making the prediction of extreme events particularly challenging. In this work, we introduce the first ordinal classification framework for forecasting wildfire severity levels directly aligned with operational decision-making in France. Our study investigates the influence of loss-function design on the ability of neural models to predict rare yet critical high-severity fire occurrences. We compare standard cross-entropy with several ordinal-aware objectives, including the proposed probabilistic TDeGPD loss derived from a truncated discrete exponentiated Generalized Pareto Distribution. Through extensive benchmarking over multiple architectures and real operational data, we show that ordinal supervision substantially improves model performance over conventional approaches. In particular, the Weighted Kappa Loss (WKLoss) achieves the best overall results, with more than +0.1 IoU gain on the most extreme severity classes while maintaining competitive calibration quality. However, performance remains limited for the rarest events due to their extremely low representation in the dataset. These findings highlight the importance of integrating both severity ordering, data imbalance considerations, and seasonality risk into wildfire forecasting systems. Future work will focus on incorporating seasonal dynamics and uncertainty information into training to further improve the reliability of extreme-event prediction. All code is available at this link and will be published on GitHub.

Keywords: Machine Learning, Forest Fire Prediction, Extreme Classification

1 Introduction

Wildfires represent one of the most pressing global natural hazards, particularly in arid or forested regions with limited water resources. The American historian Stephen Pyne and French philosopher Joëlle Zask have popularized the concept of the "Pyrocene," describing an epoch in which humanity must coexist with omnipresent fires. These increasingly frequent events cause substantial economic, ecological, and human losses. In 2018, the United States spent over $3 billion on wildfire suppression alone, excluding reconstruction and economic disruption costs [1, 2, 3], while the 2025 Los Angeles wildfire resulted in an estimated $250 billion in damages. Beyond immediate destruction, wildfires cause long-term health effects due to smoke and fine particulate

*Université Marie et Louis Pasteur, CNRS, FEMTO-ST, Belfort, France. nicolas.caron@univ-fcomte.fr
†Université Marie et Louis Pasteur, CNRS, FEMTO-ST, Belfort, France. hassan.noura@univ-fcomte.fr
‡Université Marie et Louis Pasteur, CNRS, FEMTO-ST, Belfort, France. christophe.guyeux@univ-fcomte.fr
§SAD Marketing, Lille, France. b.aynes@sad-marketing.com

matter exposure [4, 5, 6, 7, 8]; for instance, the 2018 Camp Fire in California generated over $16.5 billion in health-related costs [9]. Ecologically, fires devastate habitats, with some species requiring centuries to recover; Boulanger et al. [10] estimate that 300,000 hectares of Quebec's forests may fail to regenerate after the 2023 fire season. The resulting vegetation loss intensifies soil erosion, alters hydrological cycles, and increases greenhouse gas emissions [11, 12], while socially, wildfires are perceived as one of the most tangible manifestations of climate change [13, 14].

1.1 Problem formulation

In this work, we consider the problem of predicting the future forest fire risk. We define the wildfire prediction in definition 1.

Definition 1. ***Wildfire prediction****: Predict the future risk of wildfire ignition (or a linked-value) V in a particular area A, for a particular time range T. Knowing a particular set of characteristics F, we can mathematically define the risk of wildfire as:*

$$V(A,T) = R(F(A,T))$$

where R is a particular set of functions or an algorithm that calculates the risk value.

1.2 State of the art

A difficult aspect of wildfire prediction lies in detecting extreme events, which can manifest as (i) an anomalously large number of fires or (ii) an exceptionally large burned area. As fire prediction is generally addressed with binary classification(e.g., [15, 16, 17]), the problem of anticipating extreme events is not always accessible. Nonetheless, several strategies explicitly target this challenge.

J. Koh [18] predicts monthly fire *counts* and *burned area* over the contiguous United States using gradient boosting with extreme-value–aware losses. For counts, they use a discrete Generalized Pareto (dGPD) loss. For the burned area, they adopt a three-component mixture: a point mass at zero, a truncated log-gamma for non-extreme values, and a Generalized Pareto Distribution (GPD) for exceedance above a fixed threshold. A key limitation is this *global, fixed threshold*: fire regimes differ by region, so the same burned-area value x can be extreme in one area but typical in another, which reduces adaptability to spatial heterogeneity. Parameterization-wise, they choose a high quantile κ (used to reparameterize the GPD so that the scale depends on co-variates and is learned by boosting), assume a positive tail, and treat the GPD shape ξ as a tunable hyperparameter selected by validation; the scale is feature-dependent and estimated by the model.

Cisneros et al [19] model wildfire *occurrence* and *severity* across irregular Australian districts with a deep graph-based regression. A GCNN handles spatial adjacency and predicts occurrence (logistic) as well as the scale $\sigma(s,t)$ of an *extended* GPD (eGPD) for burned-area magnitudes. Unlike Koh's approach, no hard threshold is set: the eGPD links the bulk and the tail in a single distribution. In their specification, $\sigma(s,t)$ depends on covariates via the GCNN (model's prediction), whereas κ (a distributional quantile parameter) and ξ (tail shape) are kept constant

across space–time and chosen during model selection (learned by the model with gradient descent but are common for all disctrict).

1.3 Contribution

Our contribution to the state of the art lies in the study of the influence of loss functions within an ordinal learning framework for predicting extreme wildfire events — a crucial aspect that has not been addressed in the existing literature. We compared the performance with the EGPD-based modeling approach introduced in the literature for the same ordinal prediction framework, specifically through the proposed TDeGPD (Truncated Discrete Exponentiated Generalized Pareto Distribution) loss function. Our results demonstrate a clear advantage in using the WKLOSS function, which improves prediction accuracy on extreme classes by approximately 0.1. Despite this key improvement, we observe that achieving exact class prediction remains a major challenge and an important issue to address in future work. Our study is grounded in practice, leveraging a dataset tailored to the operational organization of emergency services in France. Figure 1 illustrates the global pipeline built in this study.

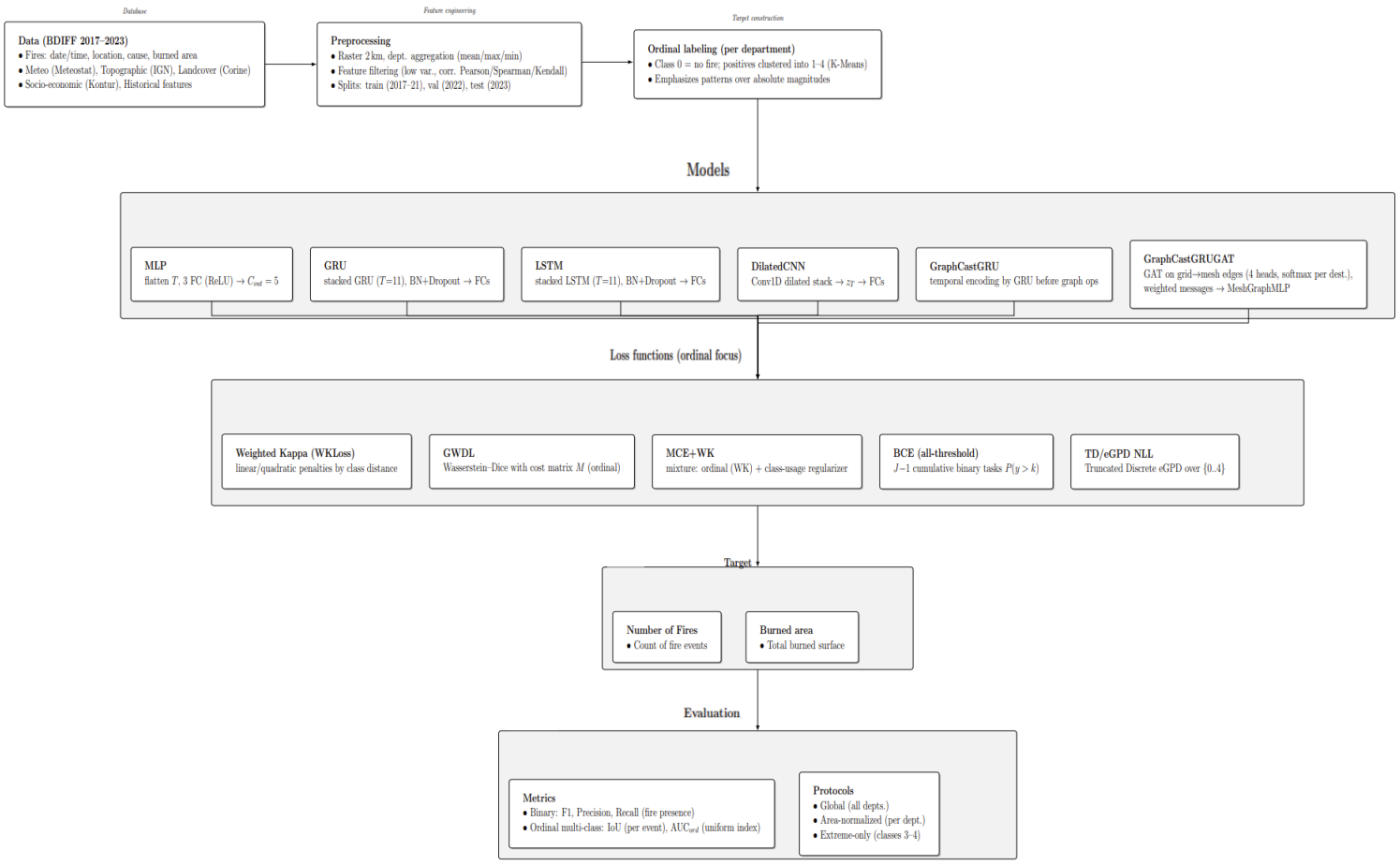

Figure 1: Diagram of the proposed study.

2 Database Construction

This section introduces and discusses the data source employed to gather wildfire-related information. It also provides details on the features and the target variable used for prediction.

2.1 The Forest Fire Database

Known as BDIFF, this online platform was created to compile all data concerning forest fires across French territory since 2006 and to make these records accessible to both the public and governmental services. The database integrates various types of information related to forest fires, including:

- Date of occurrence
- Time when the alert was issued
- Closest city
- Identified cause (criminal, accidental, etc.), when available
- Burned area
- Meteorological conditions

For this work, data covering the period from 2017 to 2023 were utilized.

2.2 Features and Target

The computation of both features and the targets variable follows the methodology described by Caron et al. [20].

The wildfire prediction task is formulated as an ordinal multi-class classification problem. For each French department, a 5-level ordinal signal of fire occurrence is defined using the K-Means clustering algorithm. Samples with zero recorded fires are assigned to class 0, while positive occurrences are divided into four clusters corresponding to Normal, Medium, High, and Extreme fire occurrence levels. This procedure emphasizes representative patterns instead of absolute magnitudes.

The variables used to train the predictive models are organized into four main groups, as detailed in Table 1: Meteorological, Topographic, Socio-Economic, and Historical. The preprocessing steps mirror those in the referenced study: data are converted into a 3D raster with a 2 km spatial resolution, aggregated by department using mean, maximum, and minimum operations, and features exhibiting low variance or strong correlation are discarded based on Pearson, Spearman, and Kendall correlation coefficients (retaining the variable with the highest variance).

The dataset is divided into three subsets: training (2017–2021), validation (2022–2024), and testing (2023). All feature engineering and statistical procedures are performed on the training data and then applied to the entire dataset. Each record in the final table represents the aggregated features and the corresponding fire risk level for a given spatial cluster within a French department. Two different targets were considered: fire occurrence (FO) and burned area (BA). As mentioned in the original article, clustering the burned area results in a much

Table 1: Summary of features used in this study. '-' means the same as above.

Variables	Frequency	Type	Source	Variables	Frequency	Type	Source
Meteorological				**Topographic**			
Temperature	12h,16h	numeric	Meteostat	Elevation	Static	numeric	IGN
Dew Point	-	-	-	Forest landcover	-	categorical	BDForet (IGN)
Precipitation	-	-	-	Landcover	-	-	Corine
Wind Direction	-	-	-	NDVI, NDSI, NDMI, NDBI, NDWI	15 days	numeric	GEE
Wind Speed	-	-	-	Swelling-shrinking of clays	-	-	-
Precipitation in Last 24h	-	-	-				
Snow height	-	-	-				
Sum of last 7 days rain	-	-	-				
Day since last rain	12h	-	Meteostat				
Nesterov	Daily	-	Derived				
Munger	-	-	-				
KBDI	-	-	-				
Angstroem	-	-	-				
BUI, ISI, FFMC, DMC, FWI	-	-	-				
Daily Severity Rating	-	-	-				
Precipitation Index (3–9 days)	-	-	Calculated				
Socio-Economic				**Historical**			
Highway	Static	numeric	BDRoute (IGN)	Past risk	Daily	numeric	Calculated
Population	-	-	Kontur	Past risk BA	-	-	-
Calendar	Daily	datetime	-	Cluster	Static	categorical	-
				Department	-	-	-

more unbalanced pattern than the occurrence of fires, mainly due to extreme values that drive the clustering process to produce very few classes other than 0 or 1. To address this issue, we propose applying the clustering on the square root of the burned area (similar to the approach used in [19], a scheme that has shown better performance in predicting extreme values compared to the baseline method.

The diagram 2 illustrates the difference between ordinal and nominal classification systems. On the left, the *ordinal classification* shows categories that follow a logical order or ranking. The scale ranges from 0 to 4, where 0 represents no fire and 4 represents an extreme number of fires and burned area. Each level corresponds to increasing severity, meaning that the categories are ordered (one value is greater or smaller than another). This type of classification is quantitative in nature, although the intervals between levels are not necessarily equal. The note "Calculated per department" indicates that this classification is applied independently for each region or department.

On the right, the *nominal classification* displays unordered categories. The classes (0–4) are used as labels only, without implying any hierarchy or magnitude between them. This type of classification is qualitative, typically used when data represent distinct groups or identifiers rather than levels of intensity.

In summary, an ordinal classification uses ranked categories (e.g., from low to high severity), while a nominal classification consists of unordered labels used simply to distinguish between categories.

2.3 Created the ordinal Scheme

We evaluated clustering performance using three methods: K-Means (from the original paper), Gaussian Mixture Models (GMM), and the EGPD-based approach. To compare the clustering

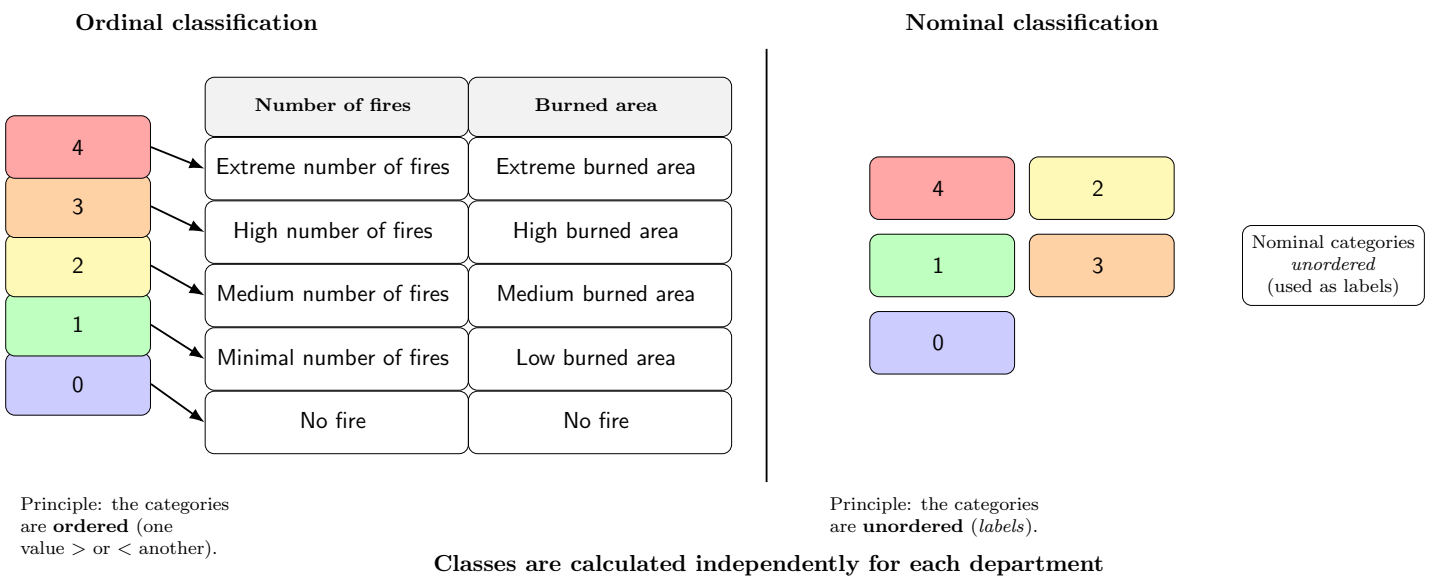

Figure 2: An ordinal schema is built in the database. Each class represents a number of fires in each department y, with $y_0 < y_1 < y_2 < y_3 < y_4$.

techniques, we relied on the Silhouette Score, as reported in Table 2.

The `eGPDRisk` approach is an ordinal clustering model based on the extended Generalized Pareto Distribution (eGPD). Zero-valued observations are treated as a separate category (Class 0), while strictly positive values are modeled using an eGPD parameterized by σ, κ, and ξ. These parameters are estimated through maximum likelihood using a two-step optimization procedure: (i) an initial Nelder–Mead exploration, followed by (ii) a constrained refinement using the L-BFGS-B algorithm with bounds enforced for numerical stability.

Once the parameters are fitted, the ordered risk thresholds are computed as theoretical or discretized quantiles of the fitted eGPD cumulative distribution function. By default, the quantiles used are:

$$q = (0.30,\ 0.60,\ 0.90).$$

These quantiles define four increasing risk classes for strictly positive observations (Classes 1–4), resulting in a total of five ordinal categories including the zero class.

The results indicate that applying clustering on the square root of the burned area yields a substantial improvement compared to clustering performed on the raw burned-area values. For the number of fires, the differences between methods are minimal. We adopted K-MEANS to remain consistent with the methodology presented in the original study.

Table 2: Silhouette Scores obtained for each target variable and clustering method. Values are rounded to two decimals.

Target	**eGPD**	**GMM**	**K-Means**
Burned Area	0.92	0.92	0.92
Burned Area (Root)	0.94	0.94	0.94
Fire Occurrence	0.98	1.00	1.00

Figure 4 compares the raw fire signal with the ordinal classification created from historical

data. The advantage of using a classification approach instead of a regression model lies in the discrete nature of fires (0 indicating no fire and a positive value otherwise). The number of fires is quite random, especially on extreme days, and the high variance of the raw signal tends to limit the convergence of predictive models. By reformulating the problem as a classification task, days with similar risk levels are grouped, which reduces variance and increases the number of days categorized as "high" or "extreme."

Figure 3 compares class distributions between the Mediterranean basin and the rest of France. Across both Mediterranean and non-Mediterranean regions, the distribution analysis shows that the fire occurrence classes follow a clear ordinal progression: higher classes consistently correspond to a greater number of fires, with Mediterranean areas exhibiting substantially higher counts in the upper-risk categories. However, when examining burned area, the separation between classes becomes much less distinct, with extensive variability and extreme outliers even within moderate classes, indicating that a small number of ignition events can still lead to severe damage. Additionally, the dominance of class 0 in both variables highlights the strong imbalance in wildfire data, while the greater representation of classes 3–4 in Mediterranean zones reinforces the heightened vulnerability of these regions. Overall, these findings emphasize that the ordinal structure of fire occurrence is well represented in the class design, whereas burned area remains far more stochastic, motivating the need for learning strategies capable of handling class imbalance and extreme-value behavior in wildfire prediction.

3 Models

In this section, we present the AI models' architecture used for evaluating the ordinality scheme, along with the precision on the different loss functions. The data imbalance problem was addressed by testing various proportions of class 0, starting from 15% to 100%, with a step of 5%. The percentage selected maximizes the Intersection over Union on the validation set. Figure 5 shows the model family types used in this study.

3.1 MLP

We consider a multilayer perceptron (MLP) (figure 6) that maps an input tensor $X \in \mathbb{R}^{B\times C_{\text{in}}\times T}$ (with B batches, C_{in} input channels, and T sequences) to an output in $\mathbb{R}^{B\times C_{\text{out}}}$. The model first flattens the temporal and channel dimensions, reshaping X to $\mathbb{R}^{B\times(C_{\text{in}}\cdot T)}$, then applies three fully connected layers with ReLU activations: $\mathbb{R}^{C_{\text{in}}\cdot T} \to \mathbb{R}^{h_{d1}}$, $\mathbb{R}^{h_{d1}} \to \mathbb{R}^{h_{d2}}$, and $\mathbb{R}^{h_{d2}} \to \mathbb{R}^{e_c}$, followed by a final linear "output" layer $\mathbb{R}^{e_c} \to \mathbb{R}^{C_{\text{out}}}$. The default configuration uses $T = 1$, $h_{d1} = 128$, $h_{d2} = 256$, $e_c = 64$, and $C_{\text{out}} = 5$, with ReLU as the internal activation throughout.

3.2 GRU

We consider a stacked Gated Recurrent Unit (GRU) (figure 7) network that processes an input tensor $X \in \mathbb{R}^{B\times C_{\text{in}}\times T}$, where B denotes the batch size, C_{in} the number of input channels, and T the number of temporal sequences. The GRU consists of a configurable number of stacked layers (`num_layers`), each with hidden size g_r, and optional inter-layer dropout with probability $p =$ `dropout`. From the final GRU layer, only the hidden state at the last time step $h_T \in \mathbb{R}^{B\times g_r}$ is

(a)

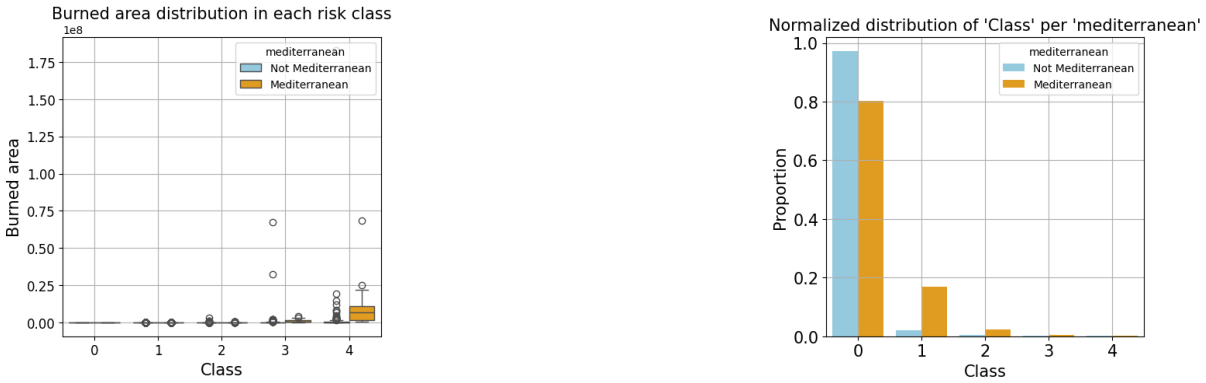

(b)

Figure 3: Distribution of FO (a) and BA-rooted (b) classes risk in the Mediterranean basin and the rest of France. Histograms have been computed relative to the category -Mediterranean (orange) or not (blue).

extracted as the temporal output. This output is normalized using batch normalization, followed by dropout with rate p. A fully connected layer then maps $\mathbb{R}^{g_r} \to \mathbb{R}^{h_d}$, followed by an activation function `act_func` (e.g., ReLU). Then another linear layer $\mathbb{R}^{h_d} \to \mathbb{R}^{e_c}$ with the same activation. Finally, an output l ayer maps $\mathbb{R}^{e_c} \to \mathbb{R}^{C_{\text{out}}}$. Default hyperparameters are $T = 11$, $g_r = 128$, `num_layers` $= 2$, $h_d = 256$, $e_c = 64$, $C_{\text{out}} = 5$, and `dropout` $= 0.03$, with ReLU used as the internal activation function.

3.3 LSTM

We consider a stacked Long Short-Term Memory (LSTM) (figure 8) network that processes an input tensor $X \in \mathbb{R}^{B \times C_{\text{in}} \times T}$, where B is the batch size, C_{in} the number of input channels, and T the number of temporal sequences. The LSTM consists of a configurable number of stacked layers (`num_layers`), each with a hidden size l_s, and optional inter-layer dropout with probability $p =$ `dropout`. From the final layer, only the hidden state at the last time step $h_T \in \mathbb{R}^{B \times l_s}$ is extracted as the temporal output. This output is normalized using batch normalization, followed by dropout with rate p. A fully connected layer then maps $\mathbb{R}^{l_s} \to \mathbb{R}^{h_d}$, followed by an activation function `act_func` (e.g., ReLU). Then another linear transformation $\mathbb{R}^{h_d} \to \mathbb{R}^{e_c}$ with the same activation. Finally, an output layer maps $\mathbb{R}^{e_c} \to \mathbb{R}^{C_{\text{out}}}$. Default hyperparameters are $T = 11$,

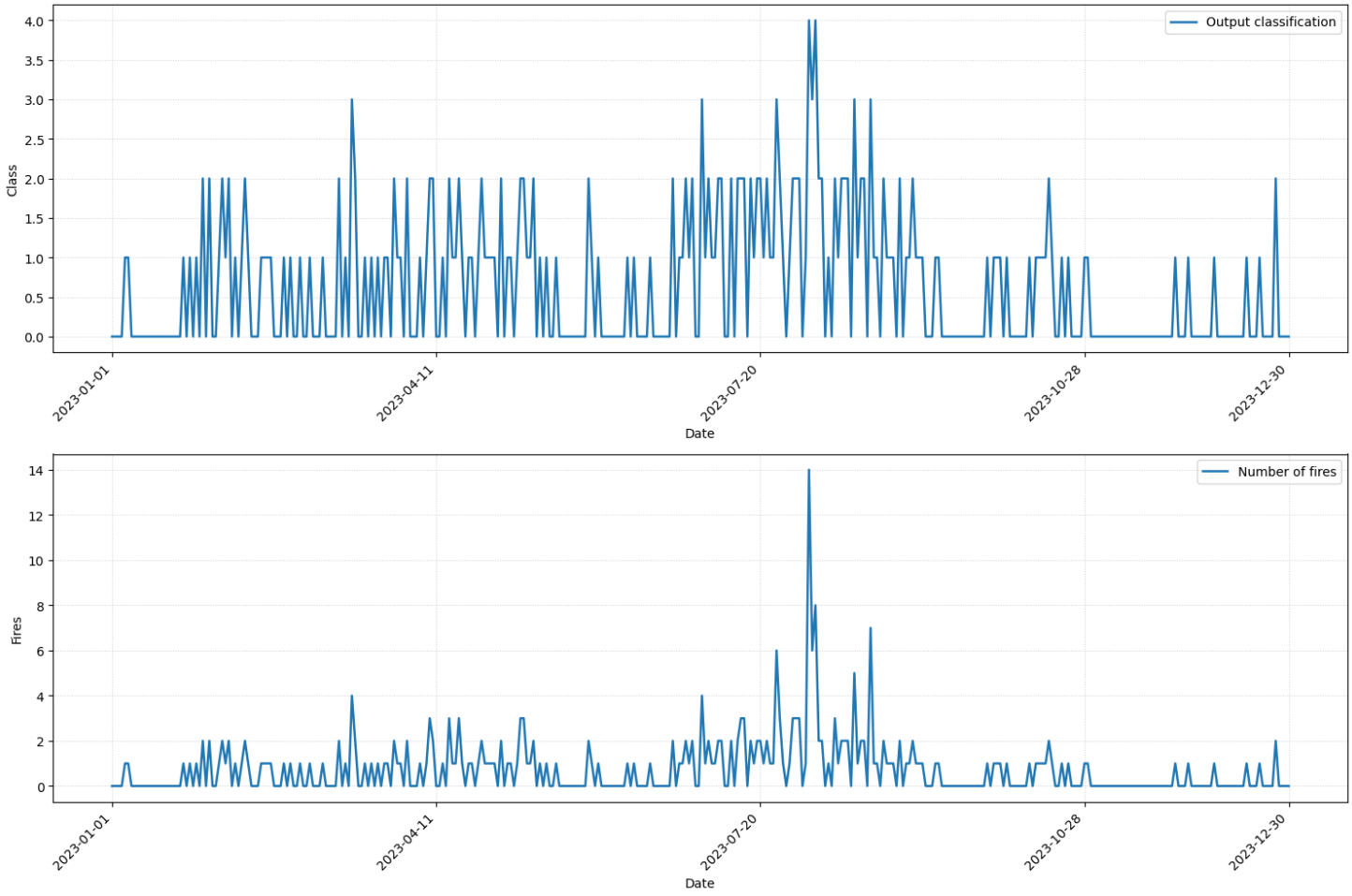

Figure 4: Comparison between the raw fire signal and the classification produced by K-Means in the Bouches-du-Rhône for the year 2023.

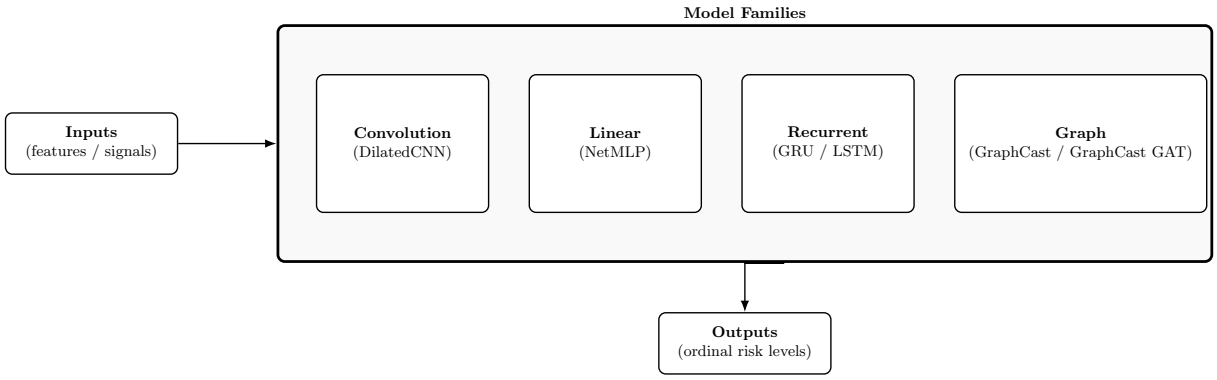

Figure 5: Models family type used in this study.

$l_s = 128$, `num_layers` $= 1$, $h_d = 256$, $e_c = 64$, $C_{\text{out}} = 5$, and `dropout` $= 0.03$, with ReLU used as the internal activation function.

3.4 DilatedCNN

We consider a temporal 1D *dilated* convolutional network (figure 9) that maps an input tensor $X \in \mathbb{R}^{B \times C_{\text{in}} \times T}$ (batch size B, input channels C_{in}, sequence length T) to an output in $\mathbb{R}^{B \times C_{\text{out}}}$.

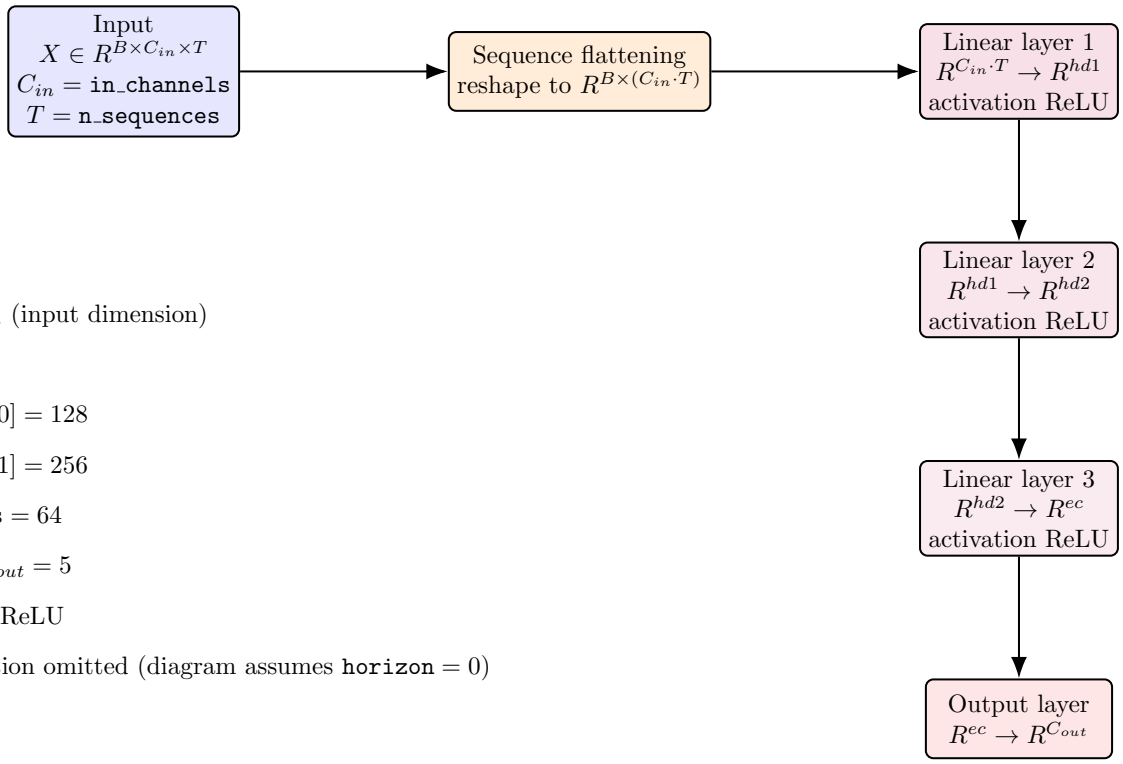

Default parameters:

- in_channels = C_{in} (input dimension)
- n_sequences = 1
- hd1 = hidden_dim[0] = 128
- hd2 = hidden_dim[1] = 256
- ec = end_channels = 64
- out_channels = C_{out} = 5
- Internal activation ReLU
- Horizon concatenation omitted (diagram assumes horizon = 0)

Figure 6: MLP neural network used in this article.

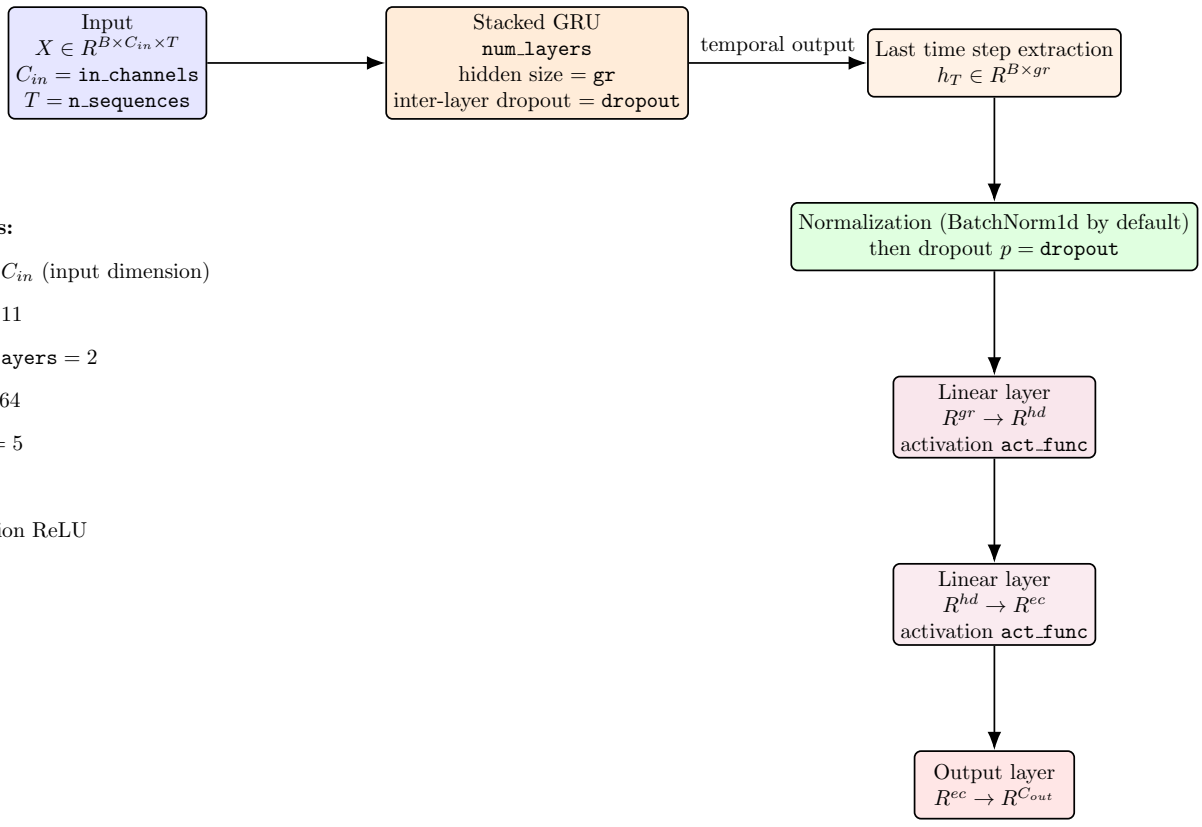

Default parameters:

- in_channels = C_{in} (input dimension)
- n_sequences = 11
- gr = 128, num_layers = 2
- hd = 256, ec = 64
- out_channels = 5
- dropout = 0.03
- Internal activation ReLU

Figure 7: GRU neural network used in this article.

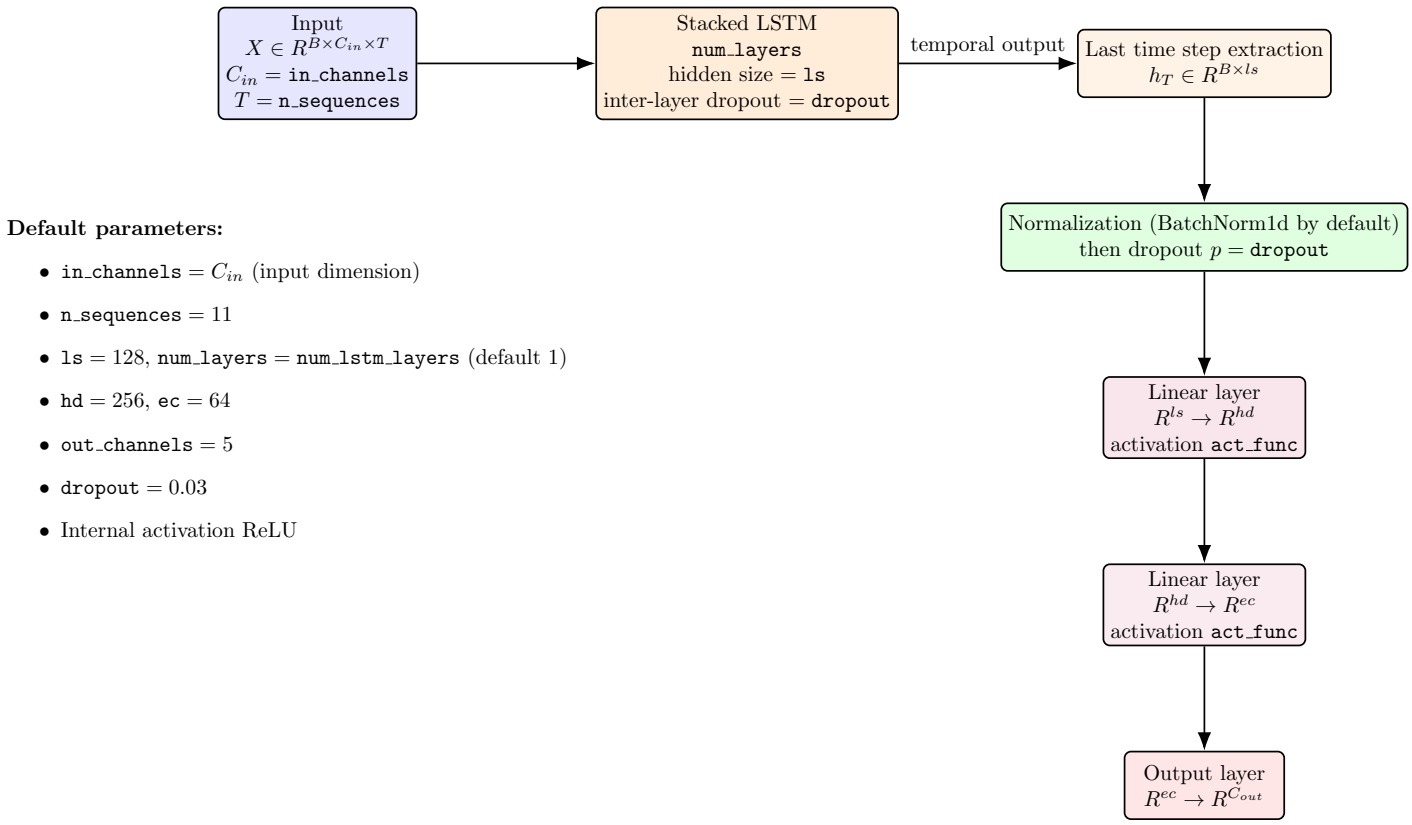

Figure 8: LSTM neural network used in this article.

The backbone is a stack of dilated Conv1D blocks configured with channel sizes **ch** and dilation rates **di**; each block applies `Conv1d` followed by `BatchNorm1d`, an activation function (ReLU by default), and dropout with probability p. From the final block, we extract the feature at the last time step $z_T \in \mathbb{R}^{B \times C_{\text{ch\_last}}}$, which is fed to a linear layer $\mathbb{R}^{C_{\text{ch\_last}}} \to \mathbb{R}^{l_c}$, an activation `act_func`, and a second linear layer $\mathbb{R}^{l_c} \to \mathbb{R}^{e_c}$ with the same activation. An output head then maps $\mathbb{R}^{e_c} \to \mathbb{R}^{C_{\text{out}}}$, with the final activation chosen according to the task. By default, $T = 11$, $\mathbf{ch} = [C_{\text{in}}, C_{\text{in}}, 128]$ with dilations $\mathbf{di} = [1, 3, 4]$, $C_{\text{ch\_last}} = 128$, $l_c = 256$, $e_c = 64$, $C_{\text{out}} = 5$, and $p = 0.03$, using ReLU as the internal activation.

3.5 GraphCast

GraphCast (figure 10 is a graph-to-grid model that encodes node features on both a regular grid and an unstructured mesh ($X_{\text{grid}} \in \mathbb{R}^{N_{\text{grid}} \times C_{\text{in}}}$, $X_{\text{mesh}} \in \mathbb{R}^{N_{\text{mesh}} \times 3}$), and propagates information through directed edges of three types: grid→mesh, mesh (intra-mesh), and mesh→grid. The architecture follows an encoder–processor–decoder scheme composed of MLP layers with Layer Normalization and SiLU activations, message aggregation by summation, and a processor consisting of multiple repeated core blocks (one encoder, four cores, and one decoder), followed by a final projection to 256 grid outputs. Communications between nodes are managed by MLPs through a *message passing* mechanism: at each layer, every node sends a "message" along its edges, where a small neural network (an MLP) computes the message from the source node's state and the edge attributes. The messages received by a target node are aggregated (here, via

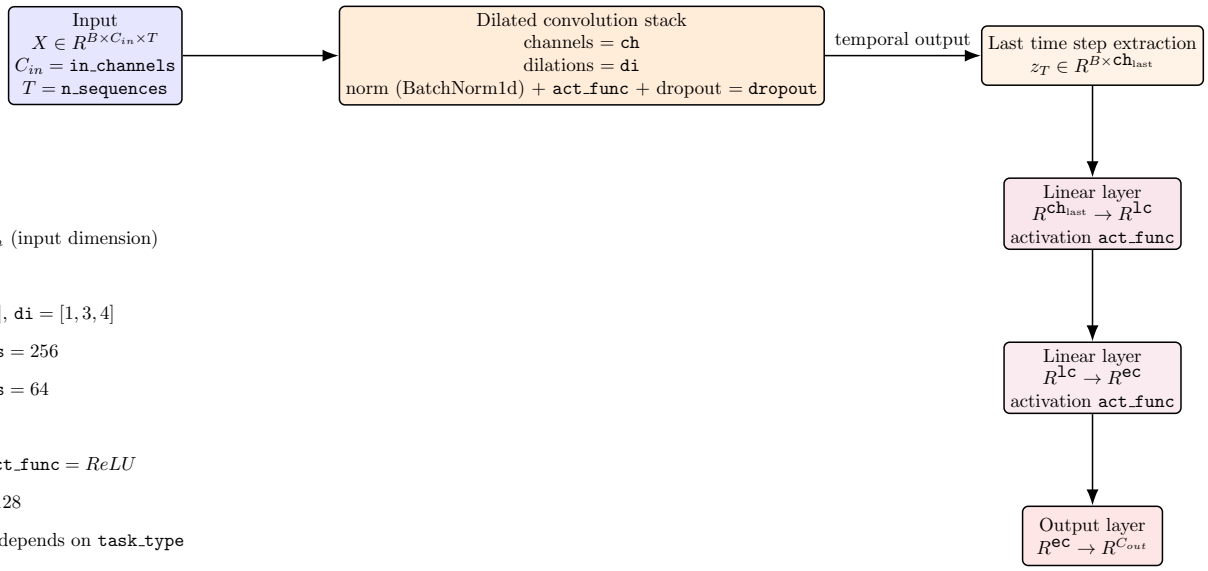

Default parameters:

- `in_channels` $= C_{in}$ (input dimension)
- `n_sequences` $= 11$
- `ch` $= [C_{in}, C_{in}, 128]$, `di` $= [1, 3, 4]$
- `lc` $=$ `lin_channels` $= 256$
- `ec` $=$ `end_channels` $= 64$
- `out_channels` $= 5$
- `dropout` $= 0.03$, `act_func` $= ReLU$
- $\texttt{ch}_{\text{last}} = \texttt{ch}[-1] = 128$
- Output activation depends on `task_type`

Figure 9: DilatedCNN neural network used in this article.

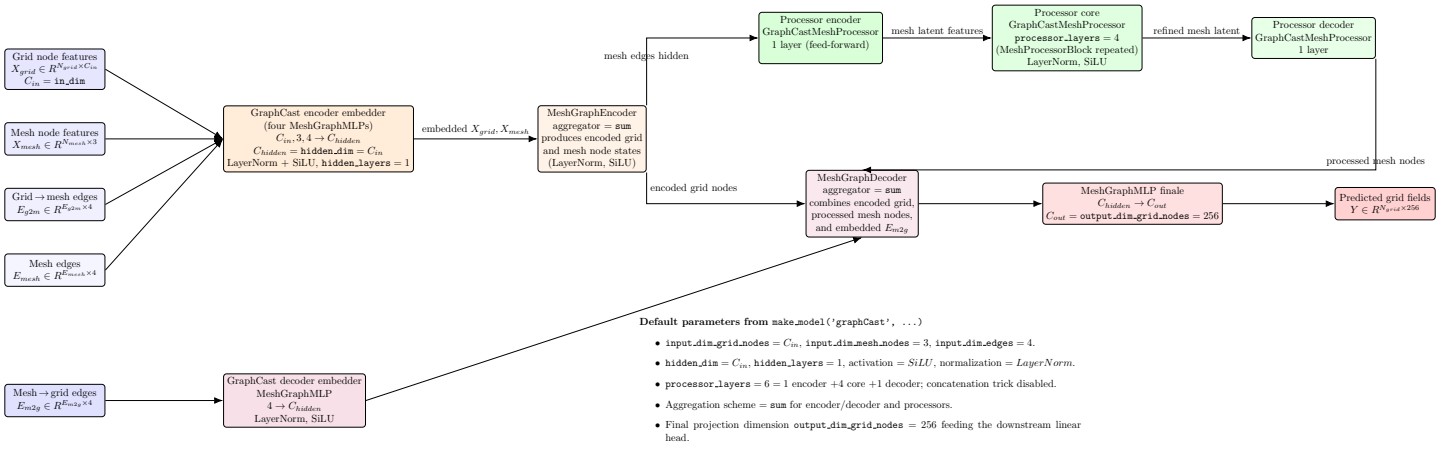

Figure 10: Main graphCast architecture

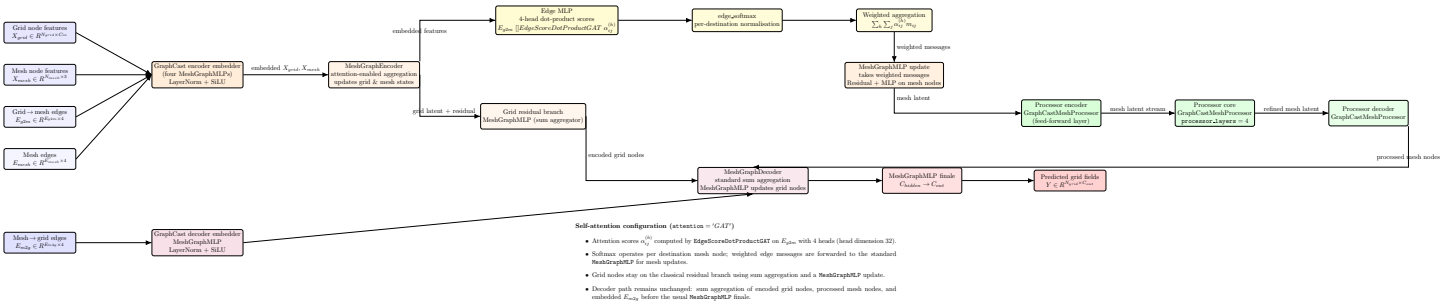

Figure 11: Main graphCast with GAT encoding architecture

summation) and passed through another MLP to update its latent state. This iterative process allows information to propagate across the graph structure, enabling the model to refine and enrich node representations before decoding back onto the grid.

3.5.1 GraphCastGRU

Michail et al. [21] implement a version of graphcast where the received features by the main models are firstly encoded with a convLSTM to take into account the temporal aspect and to reduce the computation time between nodes. In this work, we employed a similar process, replacing the convLSTM layer with a GRU layer, taking the last temporal step encoding. Figure 10 shows the main architecture of graphcast employed in this article. The output is finally given by 3 Linear layers that follow the same than the other models implemented.

3.5.2 GraphCastGRUGAT

The model can be interpreted as a modified version of the original GraphCast architecture, in which the standard sum aggregation on the grid $\rightarrow$ mesh edges is replaced by a multi-head attention mechanism (see figure 11). Structurally, the encoder–processor–decoder pipeline and the MeshGraphMLP blocks remain unchanged, but instead of summing all incoming messages equally, each message from a source node i to a target node j is weighted by an attention coefficient $\alpha_{ij}^{(h)}$, computed by the EdgeScoreDotProductGAT module (with four attention heads) and normalized via a per-destination softmax. The weighted messages are then passed through the standard MLP to update the mesh node states, while the grid branch and final decoder continue to use simple sum aggregation.

The addition of attention enables the model to adaptively focus on the most relevant neighbors, reducing noise and improving information transfer when spatial relationships or data quality vary. This makes the message passing context-dependent, potentially improving accuracy in heterogeneous regions and providing a degree of interpretability through the attention weights α, which indicate where the model "looks". Similarly, the input of the main architecture is firstly processed by a GRU layer.

4 Losses

In this section, we first detail the challenges of modeling the number of extreme fires using a probabilistic distribution, and then present the different loss functions employed within the multi-class ordinal classification framework.

4.1 Multi-class ordinal classification

In multi-class classification, models are typically trained with the cross-entropy loss in equation 1.

$$\mathcal{L}_{\mathrm{CE}}(y, \mathbf{p}) \;=\; -\sum_{c=1}^{C} \mathbf{1}[y = c] \;\log p_c, \tag{1}$$

which encourages the model to place high probability p_y on the true class y. However, for ordinal problems—where the classes have a natural order (e.g., the number of fires)—cross-entropy is not ideal because it treats all mistakes equally: any incorrect prediction contributes the same $-\log p_y$ regardless of how far the predicted class is from the true one. In other words, predicting class 0 instead of class 4 is penalized the same way as predicting class 3 instead of 4, whereas we would prefer errors that are "closer" to the true class (e.g., $1, 2$, or 3 for a true class 4) to incur a smaller penalty.

To address this, one can use loss functions tailored to ordered labels. This article compares four such objectives: *Weighted Kappa* (WKLoss), *Mean Squared Weighted Kappa* (MCEWK), *Binomial Cross-Entropy* (BCE, as implemented in the `dlordinal` [22] library), and the *Generalized Wasserstein Dice Loss* (GWDL).

4.2 WKLoss

WKLoss is designed for ordinal classification, where mistakes farther from the true class should be penalized more heavily. Let N be the batch size and J the number of classes. With model outputs $\hat{\mathbf{p}} \in \mathbb{R}^{N\times J}$ (probabilities; logits are softmaxed internally) and one-hot targets $\mathbf{Y} \in \{0,1\}^{N\times J}$, define the weighted confusion $\mathbf{C} = \hat{\mathbf{p}}^{\top}\mathbf{Y}$, and the marginals $\mathbf{h}_a = \sum_{k=1}^{N} \hat{\mathbf{p}}_{k\cdot}$ and $\mathbf{h}_b = \sum_{k=1}^{N} \mathbf{Y}_{k\cdot}$. Given a penalization matrix $\boldsymbol{\omega}$ that grows with class distance in equation 2, the loss compares the *observed* weighted disagreement to the *expected* disagreement under independence with equation 3

$$\begin{aligned} \omega_{i,j} &= \frac{|i-j|}{J-1} \qquad \text{(linear)}, \\ \omega_{i,j} &= \frac{(i-j)^2}{(J-1)^2} \quad \text{(quadratic)}. \end{aligned} \tag{2}$$

$$\mathcal{L}_{\mathrm{WK}}(\hat{\mathbf{p}}, \mathbf{Y}) = \frac{\displaystyle\sum_{i=1}^{J}\sum_{j=1}^{J} \omega_{i,j}\, C_{i,j}}{\displaystyle\frac{1}{N}\sum_{i=1}^{J}\sum_{j=1}^{J} \omega_{i,j}\, h_{a,i}\, h_{b,j} \;+\; \varepsilon}. \tag{3}$$

This yields $\mathcal{L}_{\mathrm{WK}} = 0$ for perfect predictions, values near 1 for random predictions, and up to

≈ 2 for maximally discordant outputs (as implemented). Optional class weights can be absorbed into $\boldsymbol{\omega}$. By scaling penalties with $|i-j|$, WKLoss favors "near-miss" predictions (e.g., predicting class 3 instead of true class 4) over distant errors (e.g., predicting 0 instead of 4), aligning optimization with the ordinal structure.

4.3 GWDL

GWDL [23] is designed for problems with an ordered or semantically structured label space. It replaces the binary notion of right/wrong by measuring *how far* a prediction is from the truth via a *cost matrix* $M \in \mathbb{R}^{C\times C}$ with zero diagonal, where $M[\ell, c]$ is the penalty for confusing the true class ℓ with class c. Let $\mathbf{p}_i = (p_{i,1}, \ldots, p_{i,C})$ be the predicted probabilities for sample i (softmax of logits if applicable) and y_i its true class. The per-sample Wasserstein error and the total error are given in (4):

$$\delta_i \;=\; \sum_{c=1}^{C} M[y_i, c]\; p_{i,c}, \qquad \text{TotalError} \;=\; \sum_{i=1}^{N} \delta_i. \tag{4}$$

With a designated background class b, define $w_i = M[y_i, b]$. The weighted "semantic true positives" term is defined in (5):

$$\text{TP}_w \;=\; \sum_{i=1}^{N} w_i \,\big(w_i - \delta_i\big). \tag{5}$$

The Wasserstein–Dice score and the loss are given in (6):

$$\text{Score} \;=\; \frac{2\,\text{TP}_w}{2\,\text{TP}_w + \text{TotalError} + \varepsilon}, \mathcal{L}_{\text{GWDL}} \;=\; 1 - \text{Score}. \tag{6}$$

By constructing M with an ordinal aspect, GWDL penalizes "far" mistakes more than "near" ones, aligning optimization with the ordered nature of the labels.

The effectiveness of GWDL hinges on the choice of M. Crafting M manually to reflect domain-dependent proximities (e.g., linear or quadratic distances, asymmetric penalties, background weighting) requires careful tuning. Alternatively, learning or searching M automatically (e.g., grid or Bayesian search, meta-optimization) introduces a substantial computational overhead and can prolong training. In our study, we evaluated multiple candidate matrices and retained the one that yielded the most satisfactory empirical results (shown in 7).

$$\mathbf{M} = \begin{bmatrix} 0 & 1 & 2 & 3 & 4 \\ 1 & 0 & 0.25 & 0.33 & 0.5 \\ 2 & 1.25 & 0 & 0.25 & 0.33 \\ 3 & 1.5 & 1.0 & 0 & 0.33 \\ 4 & 2 & 1.5 & 1.0 & 0 \end{bmatrix} \tag{7}$$

4.4 MCE + WK Loss.

This composite objective combines a Kappa-based ordinal loss with a class-presence regularizer. Given predictions $\hat{\mathbf{y}}$ and ground-truth labels y in equation 8:

$$\begin{aligned} \mathcal{L}_{\mathrm{MCEWK}}(\hat{\mathbf{y}}, \mathbf{y}) = C\, \mathcal{L}_{\mathrm{WK}}(\hat{\mathbf{y}}, \mathbf{y}) + (1 - C)\, \mathcal{L}_{\mathrm{MCE}}(\hat{\mathbf{y}}, \mathbf{y}) \\ C \in [0, 1]. \end{aligned} \tag{8}$$

Here, $\mathcal{L}_{\mathrm{WK}}$ is the (linear or quadratic) *Weighted Kappa* loss that increases the penalty with ordinal distance between predicted and true classes, thereby encouraging "near" mistakes over "far" ones. The $\mathcal{L}_{\mathrm{MCE}}$ term complements this by discouraging *class omission* (mode collapse), acting as a class-usage regularizer so that the model does not systematically ignore rare classes. The scalar C controls the trade-off: C=1 reduces to pure ordinal optimization via $\mathcal{L}_{\mathrm{WK}}$, while C=0 emphasizes the class-presence term. The WK component uses either linear or quadratic penalization matrices (as in standard Weighted Kappa), while the MCE component prevents the predictive distribution from collapsing onto a subset of classes. Logging and plotting utilities record the evolution of C across epochs, which is helpful to diagnose the trade-off learned by the model. Similar to GWDL loss, we tested multiple C values from (0.1, 0.2, 0.5, and 0.7). We found that C=0.7 shows the best trade-off. We didn't explore further C values as the WKLOSS function is equal to MCEWK with C = 1.0.

4.5 Binomial Cross-Entropy for Ordinal Targets (All-Threshold BCE).

For an ordinal label space $\{0, \ldots, J{-}1\}$, the all-threshold formulation converts multi-class probabilities into $J{-}1$ binary tasks that ask whether the label exceeds a threshold. Let $\mathbf{z}_n \in \mathbb{R}^J$ be the logits for sample n and $\mathbf{p}_n = \mathrm{softmax}(\mathbf{z}_n)$ with components $p_{n,c}$. For each threshold $k \in \{0, \ldots, J{-}2\}$, define the target in (9) and the predicted exceedance probability in (10):

$$s_{n,k} \;=\; \mathbb{1}[\, y_n > k \,]. \tag{9}$$

$$\hat{s}_{n,k} \;=\; \mathbb{P}(y_n > k \mid \mathbf{z}_n) \;=\; 1 \;-\; \sum_{c=0}^{k} p_{n,c}. \tag{10}$$

The per-sample all-threshold BCE is the average of binary cross-entropies across thresholds (see (11)):

$$\ell_n \;=\; \frac{1}{J-1} \sum_{k=0}^{J-2} \Big[-\, s_{n,k} \,\log \hat{s}_{n,k} \;-\; (1 - s_{n,k}) \,\log\big(1 - \hat{s}_{n,k}\big) \Big]. \tag{11}$$

With optional per-sample weights w_n, the aggregated loss is given in (12):

$$\mathcal{L}_{\mathrm{BCE}} \;=\; \begin{cases} \dfrac{\sum_{n=1}^{N} w_n\, \ell_n}{\sum_{n=1}^{N} w_n}, & \text{if weights are provided,} \\[2ex] \dfrac{1}{N} \displaystyle\sum_{n=1}^{N} \ell_n, & \text{otherwise.} \end{cases} \tag{12}$$

This objective preserves the ordinal structure by supervising all cumulative comparisons

$y > k$, encouraging probability mass to shift consistently toward higher (or lower) ordered classes while retaining the stability and interpretability of standard binary cross-entropy.

4.6 Probabilistic distribution modeling

We model an ordinal target $y \in \{0, 1, \ldots, y_{\max}\}$ with a *discrete* distribution induced by a Truncated Discrete Exponentiated Generalized Pareto (TDeGPD) CDF for the strictly positive support and then **truncate** it to the finite set $\{0, \ldots, y_{\max}\}$. This can be seen as a fusion between the proposal of [18] and [19] adapted to the ordinal classification problem. The network predicts three parameters on the last channel: $\sigma > 0$ (scale), $\kappa > 0$ (exponent), and $\xi \in >0$ (shape), which are used in the following steps:

1) GPD CDF. For $y \geq 0$, scale $\sigma > 0$ and shape $\xi \in \mathbb{R}$, the GPD CDF is

$$H(y; \sigma, \xi) \; = 1 - \left(1 + \xi \tfrac{y}{\sigma}\right)^{-1/\xi} \tag{13}$$

where the $\xi \to 0$ limit recovers the exponential CDF.

2) Exponentiated GPD (eGPD) CDF for strictly positive support. Following the "family 1" extended GPD, we raise the GPD CDF to a positive power $\kappa > 0$, which flexibly re-weights the bulk vs. tail:

$$F_+(y; \sigma, \kappa, \xi) \;=\; \big[\, H(y; \sigma, \xi) \,\big]^{\kappa}, \qquad y \geq 0,\ \kappa > 0. \tag{14}$$

3) Discretization and truncation. We induce a discrete law on $\{0, 1, 2, 3, 4\}$ by differencing the CDF at *integer* points:

$$p_{\text{raw}}(y \mid \sigma, \kappa, \xi) \;=\; F_+(y{+}1; \sigma, \kappa, \xi) \;-\; F_+(y; \sigma, \kappa, \xi), \tag{15}$$

We then *truncate and renormalize* to $\{0, \ldots, 4\}$ using the normalizing constant $Z = F_+(y_{\max} + 1; \sigma, \kappa, \xi)$:

$$p_{\text{trunc}}(y \mid \sigma, \kappa, \xi) \;=\; \frac{F_+(y{+}1; \sigma, \kappa, \xi) - F_+(y; \sigma, \kappa, \xi)}{F_+(y_{\max} + 1; \sigma, \kappa, \xi)}, \tag{16}$$

4) Training objective: truncated negative log-likelihood (NLL). Given a target $y \in \{0, \ldots, 4\}$, the per–sample loss is the truncated NLL 17.

$$\ell(\sigma, \kappa, \xi \,; y) \;=\; -\log\Big(p_{\text{trunc}}(y \mid \sigma, \kappa, \xi)\Big), \tag{17}$$

The final class is the one with the maximum probability based on the three parameters.

5 Evaluation

We evaluate the models' performance on each target using 3 main metrics:

1. Binary F1 score, which measures the performance of predicting the presence of at least one fire. Additionally, we report the precision and recall scores.

2. Intersection over Union (IoU), which measures how well the predicted risk aligns with actual risk when an event occurs. IoU is well-suited for multi-class wildfire prediction as it accounts for class uncertainty and preserves class ordinality—predicting class 1 instead of 4 is penalized less than predicting 0.

3. Auoc from [24] which uses the confusion matrix to give an ordinal error, highly reliable with imbalanced data.

For each target, we report three complementary evaluations: a global evaluation computed over all departments combined, an area-normalized score evaluation computed as the area under the performance curve per department, and an extreme evaluation using only samples of 3 or 4 (predicted or true value).

$$\mathrm{ECE} = \sum_{m=1}^{M} \frac{|B_m|}{N} \left|\mathrm{acc}(B_m) - \mathrm{conf}(B_m)\right|, \tag{18}$$

where $|B_m|$ is the number of samples in bin m, N the total number of samples, $\mathrm{acc}(B_m)$ the empirical frequency in the bin, and $\mathrm{conf}(B_m)$ the mean predicted probability. A low ECE indicates good calibration: when the model predicts a probability p, the event occurs approximately p fraction of the time. This ordinal formulation provides a more informative evaluation of predicted severity distributions, particularly for models that must remain reliable in high-risk decision-making scenarios.

6 Results

- Model Performance on global metrics Tables 3 present the model performance for predicting fire occurrence (FO) and burned area (BA). We observe that models trained with the Cross-Entropy (CE) loss generally achieve competitive results but are outperformed by ordinal-based losses (such as MCEWK, GWDL, or WKLOSS) across most architectures. For instance, while CE provides balanced results in terms of F1 and AUC for both Fire Occurrence (FO) and Burned Area (BA), applying ordinal losses consistently improves the IoU and recall scores, indicating a better capacity to capture intermediate severity levels rather than forcing binary-like predictions. This effect is particularly visible for recurrent (GRU, LSTM) and convolutional (DilatedCNN) models, which show gains of about 0.01–0.02 in F1 and IoU when trained with ordinal losses. Interestingly, the only exception is the graphCastGRU model, whose performance remains roughly unchanged (or even slightly lower) with ordinal losses—suggesting that its inherent graph structure already encodes part of this ordinal information. Overall, the results highlight the clear advantage of using ordinal loss functions for both FO and BA prediction tasks, enhancing robustness and interpretability over classical CE-based training.

- Model Performance on extreme classification Table 4 presents the results obtained on extreme fire samples (classes 3 and 4), corresponding to the most severe and infrequent fire events. Under the Cross-Entropy (CE) loss, most models already reach strong results, with F1 scores ranging from 0.85 to 0.94, and precision above 0.90. However, when ordinal-based losses such as MCEWK, GWDL, and WKLOSS are applied, the overall performance further increases

Table 3: General score comparison for Fire Occurrence (FO) and Burned Area (BA) at 0-day. Blue values indicate the best score per loss (max for all metrics except AUC, where min is best). Bold values indicate the best overall score across all models and losses.

Model	FO					BA	
	F1 (bin)	Prec (bin)	Rec (bin)	IoU	AUC	BA IoU	AUC
CE							
GRU	0.40 ± 0.01	0.31 ± 0.01	0.56 ± 0.04	0.23 ± 0.0	0.70 ± 0.01	0.22 ± 0.0	0.70 ± 0.01
LSTM	0.40 ± 0.01	0.29 ± 0.01	0.61 ± 0.01	0.23 ± 0.0	0.69 ± 0.01	0.21 ± 0.0	0.69 ± 0.01
NetMLP	0.39 ± 0.01	0.31 ± 0.02	0.52 ± 0.02	0.22 ± 0.01	0.71 ± 0.01	0.20 ± 0.01	0.71 ± 0.01
DilatedCNN	0.35 ± 0.01	0.24 ± 0.01	0.61 ± 0.02	0.20 ± 0.01	0.70 ± 0.00	0.19 ± 0.01	0.70 ± 0.0
graphCastGRU	**0.43** ± 0.01	0.33 ± 0.02	0.60 ± 0.05	**0.25** ± 0.00	0.70 ± 0.01	0.18 ± 0.03	0.69 ± 0.01
graphCastGRUGAT	0.40 ± 0.02	0.32 ± 0.03	0.53 ± 0.04	0.23 ± 0.01	0.71 ± 0.01	0.18 ± 0.01	0.71 ± 0.01
MCEWK							
GRU	0.40 ± 0.01	0.30 ± 0.01	0.59 ± 0.01	0.23 ± 0.01	0.69 ± 0.00	0.21 ± 0.00	0.68 ± 0.00
LSTM	0.41 ± 0.01	0.33 ± 0.00	0.53 ± 0.01	0.23 ± 0.01	0.69 ± 0.00	0.21 ± 0.00	**0.68** ± 0.00
NetMLP	0.40 ± 0.01	0.29 ± 0.01	0.63 ± 0.01	0.23 ± 0.00	0.69 ± 0.00	0.21 ± 0.00	0.68 ± 0.00
DilatedCNN	0.38 ± 0.01	0.28 ± 0.01	0.61 ± 0.03	0.21 ± 0.01	0.69 ± 0.01	0.20 ± 0.00	0.69 ± 0.00
graphCastGRU	0.42 ± 0.01	0.32 ± 0.01	0.62 ± 0.01	0.24 ± 0.00	0.69 ± 0.01	**0.22** ± 0.01	0.69 ± 0.00
graphCastGRUGAT	0.41 ± 0.01	0.33 ± 0.02	0.57 ± 0.06	0.23 ± 0.01	0.70 ± 0.01	0.21 ± 0.01	0.69 ± 0.00
BCE							
GRU	**0.43** ± 0.01	**0.36** ± 0.01	0.52 ± 0.02	0.24 ± 0.01	**0.69** ± 0.01	**0.23** ± 0.01	0.69 ± 0.00
LSTM	0.40 ± 0.02	0.35 ± 0.02	0.46 ± 0.04	0.23 ± 0.01	0.71 ± 0.00	0.22 ± 0.00	0.70 ± 0.01
NetMLP	0.39 ± 0.00	0.29 ± 0.01	0.60 ± 0.03	0.22 ± 0.00	0.69 ± 0.02	0.21 ± 0.01	0.69 ± 0.01
DilatedCNN	0.38 ± 0.02	0.30 ± 0.02	0.53 ± 0.02	0.21 ± 0.01	0.71 ± 0.01	0.19 ± 0.01	0.71 ± 0.01
graphCastGRU	0.37 ± 0.03	0.26 ± 0.04	**0.67** ± 0.07	0.21 ± 0.03	0.69 ± 0.01	0.22 ± 0.02	0.70 ± 0.01
graphCastGRUGAT	0.36 ± 0.02	0.26 ± 0.02	0.62 ± 0.04	0.20 ± 0.02	0.70 ± 0.01	0.18 ± 0.02	0.70 ± 0.01
GWDL							
GRU	0.42 ± 0.01	0.34 ± 0.01	0.56 ± 0.03	0.24 ± 0.01	0.69 ± 0.01	0.22 ± 0.01	0.69 ± 0.01
LSTM	0.41 ± 0.00	0.33 ± 0.01	0.53 ± 0.02	0.23 ± 0.00	0.70 ± 0.00	0.21 ± 0.01	0.69 ± 0.01
NetMLP	0.41 ± 0.01	0.34 ± 0.01	0.52 ± 0.01	0.22 ± 0.00	0.69 ± 0.01	0.22 ± 0.00	0.71 ± 0.01
DilatedCNN	0.41 ± 0.00	0.32 ± 0.01	0.57 ± 0.01	0.22 ± 0.01	0.69 ± 0.01	0.21 ± 0.01	0.71 ± 0.01
graphCastGRU	0.42 ± 0.01	0.33 ± 0.01	0.56 ± 0.04	0.23 ± 0.01	0.69 ± 0.00	0.20 ± 0.01	0.69 ± 0.01
graphCastGRUGAT	0.39 ± 0.01	0.30 ± 0.05	0.60 ± 0.15	0.21 ± 0.02	0.69 ± 0.01	0.21 ± 0.00	0.70 ± 0.01
WKLOSS							
GRU	0.42 ± 0.01	0.32 ± 0.01	0.62 ± 0.01	**0.25** ± 0.01	0.68 ± 0.00	0.21 ± 0.01	**0.69** ± 0.01
LSTM	0.41 ± 0.01	0.30 ± 0.01	0.64 ± 0.01	0.23 ± 0.01	0.68 ± 0.00	0.20 ± 0.00	0.69 ± 0.00
NetMLP	0.40 ± 0.00	0.29 ± 0.01	0.65 ± 0.02	0.23 ± 0.00	**0.67** ± 0.02	0.22 ± 0.01	0.70 ± 0.00
DilatedCNN	0.40 ± 0.01	0.30 ± 0.01	0.63 ± 0.01	0.23 ± 0.01	0.68 ± 0.01	0.20 ± 0.01	0.69 ± 0.01
graphCastGRU	0.42 ± 0.01	0.32 ± 0.02	0.60 ± 0.03	0.24 ± 0.01	0.69 ± 0.01	0.20 ± 0.01	0.69 ± 0.01
graphCastGRUGAT	0.40 ± 0.01	0.29 ± 0.02	0.64 ± 0.03	0.23 ± 0.01	0.68 ± 0.00	0.21 ± 0.01	0.69 ± 0.00
TDeGPD							
GRU	0.34 ± 0.01	0.24 ± 0.01	0.60 ± 0.02	0.19 ± 0.00	0.68 ± 0.01	0.18 ± 0.00	0.71 ± 0.00
LSTM	0.32 ± 0.00	0.23 ± 0.01	0.56 ± 0.03	0.17 ± 0.01	0.70 ± 0.03	0.17 ± 0.00	0.69 ± 0.01
NetMLP	0.33 ± 0.02	0.26 ± 0.02	0.47 ± 0.03	0.18 ± 0.01	0.70 ± 0.03	0.18 ± 0.01	0.69 ± 0.02
DilatedCNN	0.35 ± 0.01	0.27 ± 0.01	0.54 ± 0.02	0.20 ± 0.00	0.70 ± 0.01	0.16 ± 0.00	0.71 ± 0.01
graphCastGRU	0.39 ± 0.04	0.29 ± 0.04	0.63 ± 0.06	0.22 ± 0.02	0.69 ± 0.01	0.21 ± 0.03	0.70 ± 0.01
graphCastGRUGAT	0.38 ± 0.01	0.28 ± 0.02	0.64 ± 0.02	0.22 ± 0.01	0.70 ± 0.01	0.20 ± 0.02	0.71 ± 0.02

Table 4: Extreme score comparison for Fire Occurrence (FO) and Burned Area (BA) at 0-day. Blue mark the best score per loss (max for all metrics except AUC, where min is best). Bold marks the best overall score across all models/losses.

Model	FO					BA	
	F1 (bin)	Prec (bin)	Rec (bin)	IoU	AUC	BA IoU	AUC
CE							
GRU	0.91 ± 0.01	0.95 ± 0.05	0.88 ± 0.04	0.35 ± 0.02	1.00 ± 0.01	0.13 ± 0.02	1.00 ± 0.00
LSTM	0.94 ± 0.02	0.99 ± 0.01	0.89 ± 0.04	0.34 ± 0.03	0.99 ± 0.01	0.14 ± 0.02	1.00 ± 0.00
NetMLP	0.85 ± 0.03	0.93 ± 0.03	0.79 ± 0.05	0.31 ± 0.01	0.99 ± 0.01	0.11 ± 0.01	1.01 ± 0.02
DilatedCNN	0.90 ± 0.02	0.96 ± 0.04	0.85 ± 0.02	0.34 ± 0.01	1.00 ± 0.01	0.11 ± 0.03	1.00 ± 0.00
graphCastGRU	0.93 ± 0.01	**1.00** ± 0.00	0.87 ± 0.02	0.32 ± 0.02	1.00 ± 0.00	0.16 ± 0.02	1.00 ± 0.00
graphCastGRUGAT	0.91 ± 0.02	0.97 ± 0.04	0.85 ± 0.03	0.32 ± 0.02	1.00 ± 0.00	0.15 ± 0.02	1.00 ± 0.00
MCEWK							
GRU	0.94 ± 0.01	**1.00** ± 0.00	0.88 ± 0.02	0.41 ± 0.02	1.00 ± 0.00	0.24 ± 0.01	1.00 ± 0.00
LSTM	0.89 ± 0.02	**1.00** ± 0.00	0.80 ± 0.04	0.37 ± 0.01	1.00 ± 0.00	0.19 ± 0.01	1.00 ± 0.00
NetMLP	0.94 ± 0.01	0.99 ± 0.03	0.90 ± 0.02	0.41 ± 0.02	1.00 ± 0.00	0.17 ± 0.01	1.00 ± 0.00
DilatedCNN	0.93 ± 0.03	**1.00** ± 0.00	0.86 ± 0.05	0.40 ± 0.03	1.00 ± 0.00	0.19 ± 0.01	1.00 ± 0.00
graphCastGRU	0.93 ± 0.01	0.98 ± 0.05	0.90 ± 0.03	**0.45** ± 0.02	1.00 ± 0.01	0.20 ± 0.02	1.00 ± 0.00
graphCastGRUGAT	0.87 ± 0.03	0.87 ± 0.07	0.88 ± 0.05	0.37 ± 0.04	1.01 ± 0.01	0.20 ± 0.03	1.00 ± 0.00
BCE							
GRU	0.89 ± 0.01	0.91 ± 0.05	0.88 ± 0.02	0.34 ± 0.02	0.99 ± 0.01	0.12 ± 0.02	1.00 ± 0.00
LSTM	0.87 ± 0.03	0.91 ± 0.04	0.83 ± 0.05	0.33 ± 0.02	1.00 ± 0.00	0.12 ± 0.01	1.00 ± 0.01
NetMLP	0.88 ± 0.01	0.92 ± 0.03	0.84 ± 0.02	0.32 ± 0.02	0.99 ± 0.01	0.11 ± 0.01	0.99 ± 0.01
DilatedCNN	0.85 ± 0.02	0.86 ± 0.05	0.83 ± 0.03	0.34 ± 0.03	1.00 ± 0.01	0.11 ± 0.02	1.01 ± 0.01
graphCastGRU	0.88 ± 0.10	0.84 ± 0.18	**0.93** ± 0.04	0.34 ± 0.05	1.00 ± 0.00	0.12 ± 0.03	1.00 ± 0.00
graphCastGRUGAT	0.88 ± 0.07	0.87 ± 0.10	0.89 ± 0.05	0.35 ± 0.05	1.00 ± 0.01	0.14 ± 0.02	1.00 ± 0.00
GWDL							
GRU	0.91 ± 0.06	0.94 ± 0.13	0.88 ± 0.03	0.43 ± 0.04	1.00 ± 0.00	0.18 ± 0.03	1.00 ± 0.00
LSTM	0.92 ± 0.01	**1.00** ± 0.00	0.85 ± 0.02	0.42 ± 0.02	1.00 ± 0.00	0.19 ± 0.03	1.00 ± 0.00
NetMLP	0.84 ± 0.09	0.85 ± 0.20	0.85 ± 0.05	0.37 ± 0.06	**0.98** ± 0.03	0.11 ± 0.02	1.00 ± 0.00
DilatedCNN	0.84 ± 0.11	0.84 ± 0.23	0.89 ± 0.05	0.38 ± 0.09	**0.98** ± 0.03	0.15 ± 0.01	1.00 ± 0.00
graphCastGRU	0.85 ± 0.11	0.84 ± 0.22	0.90 ± 0.03	0.41 ± 0.09	0.99 ± 0.01	0.20 ± 0.03	1.00 ± 0.00
graphCastGRUWithAttentionGAT	0.87 ± 0.12	0.91 ± 0.21	0.87 ± 0.12	0.36 ± 0.08	0.99 ± 0.03	0.17 ± 0.03	1.00 ± 0.00
WKLOSS							
GRU	0.95 ± 0.01	**1.00** ± 0.00	0.90 ± 0.01	**0.45** ± 0.02	1.00 ± 0.00	**0.26** ± 0.02	1.00 ± 0.00
LSTM	**0.96** ± 0.00	**1.00** ± 0.00	0.92 ± 0.01	**0.45** ± 0.02	1.00 ± 0.00	0.22 ± 0.04	1.00 ± 0.00
NetMLP	0.93 ± 0.02	0.97 ± 0.06	0.90 ± 0.01	0.41 ± 0.05	0.99 ± 0.04	0.15 ± 0.03	1.00 ± 0.00
DilatedCNN	0.95 ± 0.01	**1.00** ± 0.00	0.91 ± 0.01	0.43 ± 0.02	1.00 ± 0.00	0.21 ± 0.02	1.00 ± 0.00
graphCastGRU	0.87 ± 0.06	0.84 ± 0.12	0.92 ± 0.02	0.40 ± 0.06	1.00 ± 0.03	0.21 ± 0.04	1.00 ± 0.00
graphCastGRUGAT	0.94 ± 0.02	0.98 ± 0.04	0.91 ± 0.01	0.44 ± 0.05	1.00 ± 0.00	0.20 ± 0.03	1.00 ± 0.01
TDeGPD							
GRU	0.88 ± 0.03	0.97 ± 0.02	0.80 ± 0.05	0.35 ± 0.03	**0.98** ± 0.01	0.13 ± 0.02	1.00 ± 0.00
LSTM	0.80 ± 0.03	0.85 ± 0.04	0.75 ± 0.04	0.31 ± 0.02	1.00 ± 0.02	0.12 ± 0.02	0.99 ± 0.02
NetMLP	0.76 ± 0.05	0.77 ± 0.07	0.75 ± 0.08	0.28 ± 0.04	**0.98** ± 0.03	0.16 ± 0.03	0.99 ± 0.01
DilatedCNN	0.85 ± 0.04	0.92 ± 0.03	0.79 ± 0.06	0.35 ± 0.03	1.01 ± 0.01	0.11 ± 0.01	1.00 ± 0.01
graphCastGRU	0.94 ± 0.02	**1.00** ± 0.00	0.89 ± 0.04	0.34 ± 0.05	1.00 ± 0.00	0.13 ± 0.02	1.00 ± 0.00
graphCastGRUWithAttentionGAT	0.95 ± 0.02	**1.00** ± 0.01	0.90 ± 0.03	0.33 ± 0.04	1.00 ± 0.01	0.11 ± 0.01	1.00 ± 0.00

Table 5: Area score comparison with the area score generalization at 0-day. Blue mark the best score per loss. Bold marks the best overall score across all models/losses.

Model	FO				BA
	F1 (bin)	Prec (bin)	Rec (bin)	IoU	BA IoU
CE					
GRU	0.16 ± 0.02	0.13 ± 0.02	0.24 ± 0.04	0.09 ± 0.01	0.08 ± 0.00
LSTM	0.16 ± 0.01	0.13 ± 0.01	0.27 ± 0.01	0.09 ± 0.01	**0.09** ± 0.01
NetMLP	0.15 ± 0.01	**0.15** ± 0.01	0.22 ± 0.02	0.08 ± 0.01	**0.09** ± 0.00
DilatedCNN	0.16 ± 0.01	0.12 ± 0.01	**0.31** ± 0.03	0.09 ± 0.01	**0.09** ± 0.01
graphCastGRU	0.16 ± 0.00	0.14 ± 0.01	0.23 ± 0.04	0.09 ± 0.00	0.08 ± 0.00
graphCastGRUGAT	0.13 ± 0.01	0.12 ± 0.01	0.19 ± 0.02	0.07 ± 0.00	0.07 ± 0.01
MCEWK					
GRU	0.16 ± 0.01	0.13 ± 0.01	0.22 ± 0.01	0.09 ± 0.01	**0.09** ± 0.00
LSTM	0.14 ± 0.00	0.13 ± 0.01	0.20 ± 0.01	0.08 ± 0.01	**0.09** ± 0.00
NetMLP	0.14 ± 0.00	0.14 ± 0.01	0.20 ± 0.01	0.07 ± 0.01	**0.09** ± 0.01
DilatedCNN	0.16 ± 0.01	**0.15** ± 0.01	0.24 ± 0.01	0.09 ± 0.00	**0.09** ± 0.00
graphCastGRU	0.16 ± 0.01	0.14 ± 0.02	**0.25** ± 0.01	0.09 ± 0.01	**0.09** ± 0.00
graphCastGRUGAT	0.14 ± 0.01	0.13 ± 0.01	0.22 ± 0.04	0.08 ± 0.01	**0.09** ± 0.01
BCE					
GRU	0.14 ± 0.01	0.14 ± 0.01	0.19 ± 0.01	0.08 ± 0.00	0.08 ± 0.01
LSTM	0.13 ± 0.01	0.14 ± 0.01	0.17 ± 0.02	0.07 ± 0.01	0.08 ± 0.01
NetMLP	0.16 ± 0.02	**0.15** ± 0.02	0.26 ± 0.03	0.09 ± 0.01	0.08 ± 0.01
DilatedCNN	0.16 ± 0.01	0.14 ± 0.01	0.23 ± 0.01	0.09 ± 0.01	**0.09** ± 0.01
graphCastGRU	0.16 ± 0.01	0.13 ± 0.01	**0.32** ± 0.04	0.09 ± 0.01	0.07 ± 0.01
graphCastGRUGAT	0.16 ± 0.01	0.13 ± 0.01	0.28 ± 0.03	0.08 ± 0.01	0.08 ± 0.00
GWDL					
GRU	0.16 ± 0.01	0.13 ± 0.01	0.22 ± 0.01	0.09 ± 0.01	0.08 ± 0.00
LSTM	0.14 ± 0.00	0.13 ± 0.01	0.20 ± 0.01	0.08 ± 0.01	0.08 ± 0.01
NetMLP	0.14 ± 0.00	0.14 ± 0.01	0.20 ± 0.01	0.07 ± 0.01	0.07 ± 0.00
DilatedCNN	0.16 ± 0.01	**0.15** ± 0.01	0.24 ± 0.01	0.09 ± 0.00	0.08 ± 0.00
graphCastGRU	0.15 ± 0.00	0.14 ± 0.01	0.22 ± 0.02	0.08 ± 0.00	0.07 ± 0.00
graphCastGRUGAT	0.14 ± 0.02	0.12 ± 0.02	**0.25** ± 0.08	0.08 ± 0.02	0.07 ± 0.00
WKLOSS					
GRU	**0.17** ± 0.01	0.14 ± 0.01	0.26 ± 0.02	0.09 ± 0.01	**0.09** ± 0.00
LSTM	0.16 ± 0.01	0.13 ± 0.01	0.26 ± 0.01	0.09 ± 0.00	**0.09** ± 0.00
NetMLP	0.16 ± 0.01	0.13 ± 0.01	0.28 ± 0.01	0.09 ± 0.00	**0.09** ± 0.00
DilatedCNN	**0.17** ± 0.01	0.14 ± 0.01	0.28 ± 0.02	**0.10** ± 0.01	**0.09** ± 0.00
graphCastGRU	0.15 ± 0.02	0.14 ± 0.03	0.23 ± 0.02	0.08 ± 0.01	**0.09** ± 0.00
graphCastGRUGAT	0.15 ± 0.01	0.13 ± 0.01	0.26 ± 0.03	0.09 ± 0.01	0.08 ± 0.01
TDeGPD					
GRU	0.15 ± 0.01	0.12 ± 0.01	0.29 ± 0.01	0.09 ± 0.01	0.08 ± 0.00
LSTM	0.15 ± 0.01	0.13 ± 0.02	0.29 ± 0.02	0.08 ± 0.01	0.08 ± 0.01
NetMLP	0.14 ± 0.01	0.13 ± 0.01	0.22 ± 0.01	0.08 ± 0.01	0.08 ± 0.00
DilatedCNN	0.15 ± 0.01	0.12 ± 0.01	0.25 ± 0.03	0.08 ± 0.01	0.08 ± 0.00
graphCastGRU	0.15 ± 0.00	0.13 ± 0.01	0.27 ± 0.06	0.09 ± 0.01	0.08 ± 0.01
graphCastGRUGAT	0.15 ± 0.01	0.13 ± 0.01	0.27 ± 0.02	0.08 ± 0.01	0.07 ± 0.01

across nearly all architectures. For instance, the GRU model improves its IoU from 0.35 (CE) to 0.45 (WKLOSS) and its BA IoU from 0.13 to 0.26, while the LSTM shows a similar gain, with an F1 rising from 0.94 to 0.96 and an IoU from 0.34 to 0.45.

Importantly, the GraphCastGRU model also benefits from ordinal supervision — contrary to the global results — improving its IoU from 0.32 (CE) to 0.45 (MCEWK) and maintaining a very high F1 score around 0.93. These results indicate that ordinal losses help the model better capture the gradation between moderate and extreme fires, rather than treating them as binary events. Overall, the application of ordinal losses provides a clear advantage in detecting and characterizing high-intensity fires, with consistent improvements of +0.05 to +0.10 in IoU and up to +0.13 in BA IoU compared to the standard CE formulation.

- Model Performance on Area-Normalized Across Departments Table 5 compares model performances under different loss functions for the area generalization task at 0-day. Globally, all models obtain relatively low scores, reflecting the difficulty of generalizing fire dynamics across heterogeneous regions. Under the Cross-Entropy (CE) baseline, F1 scores remain modest ($\approx$0.13$-$0.16 for FO), IoU values around 0.08–0.09, and Burned Area IoU (BA IoU) rarely exceeding 0.09. This indicates that while models can identify regional fire patterns, they tend to overfit to the training zones and struggle to adapt spatially.

When using ordinal-based loss functions—notably MCEWK, GWDL, and WKLOSS—most architectures maintain or slightly improve their spatial generalization capacity. For instance, DilatedCNN shows a gain from 0.09 (CE) to 0.10 (WKLOSS) in IoU and a recall increase from 0.31 to 0.28 (comparable, but more stable). Similarly, the GRU model improves its recall from 0.24 (CE) to 0.26 (WKLOSS) and its BA IoU from 0.08 to 0.09, showing slightly better sensitivity to fires in unseen regions. Although the absolute improvements are small (typically +0.01 to +0.02 in F1 or IoU), they suggest that ordinal losses help regularize learning, yielding models less prone to overfitting local data distributions.

In summary, although the overall generalization scores remain low due to the intrinsic regional variability of wildfire behavior, ordinal losses consistently stabilize and modestly improve performance across architectures. They thus contribute to better spatial robustness—particularly important for transferring fire prediction models across different French departments.

- Fire Occurrence vs. Burned Area Across the three evaluation settings, models consistently achieve higher performance on FO than on BA. In the general comparison (Table 3), IoU values reach 0.25, while BA IoU remains lower, typically between 0.21 and 0.25. This discrepancy widens in the area generalization experiment (Table 5), where IoU values are still slightly better than BA IoU. These results highlight that fire occurrence, being a more frequent and binary signal, is easier to predict and generalize, whereas burned area—highly imbalanced and dominated by extreme values—remains a more complex and unstable target.

- Probabilistic Distribution Modelling The TDeGPD distribution–based modeling clearly underperforms compared to the other loss functions. In the global performance scores, TDeGPD yields noticeably lower FO, F1, and IoU values. GRU and LSTM models in particular suffer a significant drop in F1 ($\approx$0.32$-$0.35) and IoU ($\leq$ 0.20), whereas imbalance-aware losses maintain stronger performance. When looking at extreme fire events, FO performance improves somewhat under TDeGPD, with F1 scores sometimes exceeding 0.90 for graphcast-based architectures. However, the IoU still lags behind more suitable losses like WKLOSS or MCEWK. Finally, in

the area-based evaluation, the scores drop again and remain below the best-performing losses.

- Conclusion On Metrics Analysis Across all experiments, models consistently perform better on FO than on BA, reflecting the greater difficulty of predicting continuous and highly imbalanced burned-area values. In the global comparison, ordinal-based losses (MCEWK, GWDL, WKLOSS) outperform the Cross-Entropy (CE) baseline across most architectures, improving IoU and recall by about +0.01–0.03 for FO and up to +0.05–0.10 for BA. These improvements indicate that ordinal formulations help capture intermediate fire-severity levels and reduce the binary bias of standard classification. On extreme samples, ordinal losses provide the strongest benefit, particularly for GRU, LSTM, and GraphCastGRU models, where IoU increases from 0.32–0.35 (CE) to 0.45 (MCEWK/WKLOSS) and BA IoU rises from 0.13 to 0.26, confirming their ability to better model rare, high-intensity events. Among all tested loss functions, the WKLOSS (Weighted Kappa Loss) emerges as the most effective and consistent across all experiments.

6.1 Calibration analysis

Figure 12 shows the confusion matrix for FO using the CE, WKLOSS, and TDeGPD losses on the GRU model on FO. The advantage of the WKLOSS is clearly visible, as the matrix is more concentrated along the diagonal, indicating more accurate class alignment. The overall error is lower with the ordinal loss, but it still fails to produce reliable predictions for extreme classes (3 and 4). By comparing the confusion matrix of the model trained with the TDeGPD loss, we observe clear advantages over the standard Cross-Entropy formulation. First, the diagonal is noticeably more pronounced, indicating a better alignment between predicted and true classes. In addition, the model can correctly identify samples from classes 3 and 4, even though their proportion remains very small relative to the dominant lower-risk classes. This supports the idea that the TDeGPD-based formulation is well-suited for ordinal classification, and more specifically for predicting extreme wildfire events, as it can better distinguish moderate and extreme risk.

Figure 13 reports the classwise calibration plots obtained by averaging the predicted probabilities over models for three different loss functions: standard Cross-Entropy (CE), Weighted Kappa Loss (WKLoss), and the Truncated Discrete eGPD (TD-eGPD).

- Cross entropy The calibration curves reveal markedly different behaviors across the classes. Class 0 is generally well-calibrated: the predicted probabilities align reasonably well with the observed frequencies, with only a slight tendency toward overconfidence at low probability values. Class 1 shows a less accurate calibration, with underestimated low probabilities and overestimated values around 0.5. In contrast, Classes 2, 3, and 4 exhibit strong instability and poor calibration, with points deviating significantly from the diagonal. This indicates unreliable confidence estimates for these classes, mainly due to their low representation in the dataset: predicted probabilities remain close to zero and do not accurately reflect true occurrences. Overall, the model performs effectively for the majority class but demonstrates substantial limitations for minority classes.

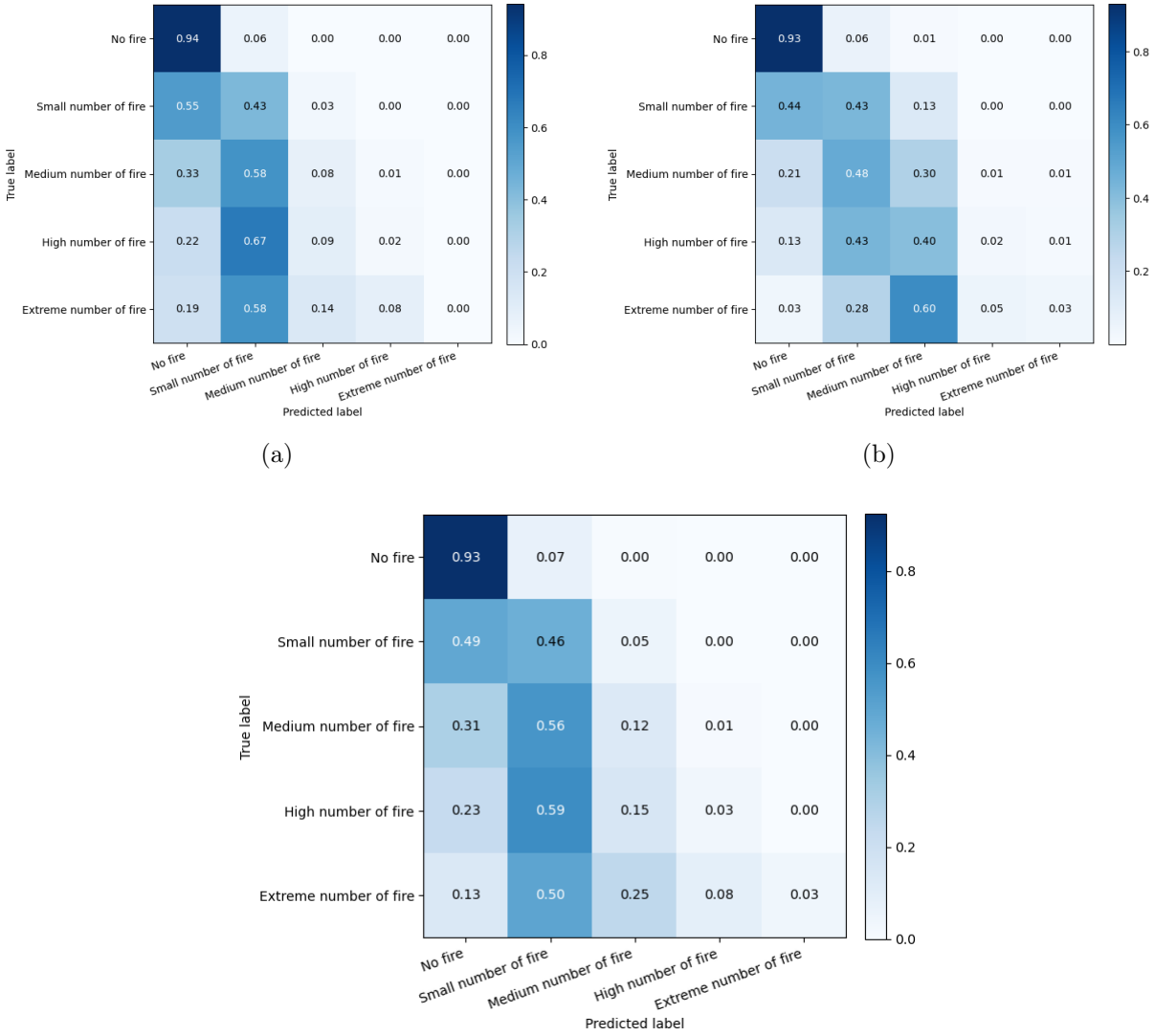

(a) (b)

(c)

Figure 12: Average Confusion matrix comparison with CE (a), WKLOSS (b), and TDeGPD (c) on FO. Matrices are normalized on true values.

- WKLOSS For the majority class (Class 0), the CE models demonstrated a reasonably good alignment with the diagonal, but the new model shows a slightly smoother and more consistent calibration, especially by reducing the overconfidence at low predicted probabilities. Class 1 also benefits from noticeable improvements: the calibration curve now more closely follows the ideal trend, with reduced bias in the mid-range. Conversely, the situation remains unfavorable for Classes 2, 3, and 4. Although the new model displays slightly higher predicted probabilities for these minority classes, the calibration curves still deviate significantly from the diagonal, indicating persistent underestimation of true frequencies and unstable confidence estimates. These results suggest that while the WKLOSS models provide better calibration for the well-represented classes, it continues to struggle with minority classes, emphasizing that the primary limitation stems from class imbalance rather than model specification alone.

- TDeGPD For Class 0, the calibration curve remains close to the diagonal, confirming that models continue to provide reliable probability estimates for the majority class. Class 1 also shows improvement, with a more linear calibration trend and reduced underestimation compared to earlier results. However, significant changes are visible for Classes 2, 3, and 4. While the previous losses tended to systematically underestimate these minority classes, the TDeGPD displays irregular and abrupt deviations from the diagonal, including instances of extreme overconfidence (e.g., predicted probabilities around 0.4–0.5 leading to observed frequencies approaching 1). These inconsistencies indicate that, although it is now more willing to assign higher probabilities to rare outcomes, it does so unreliably, resulting in poor calibration stability.

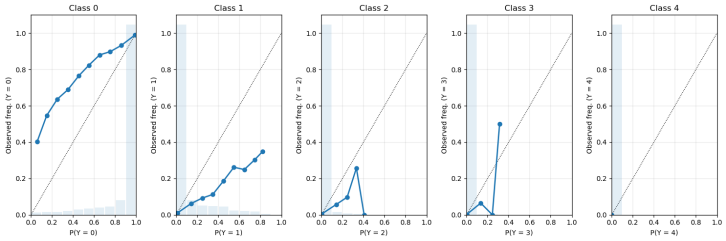

(a)

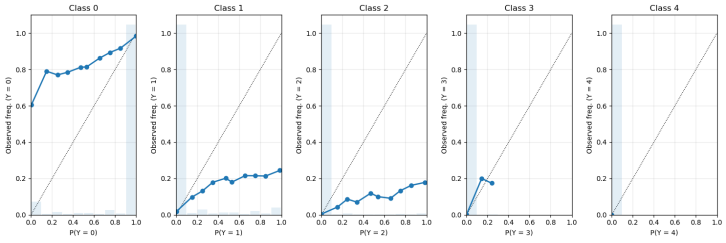

(b)

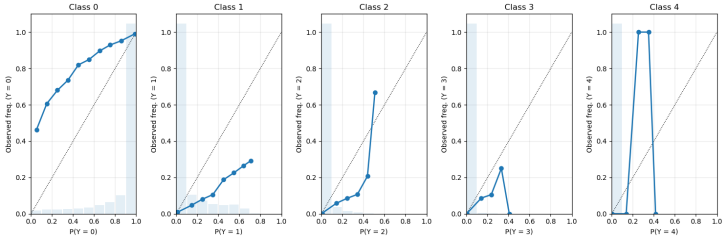

(c)

Figure 13: Average Calibration error with CE (a), WKLOSS (b), and TDeGPD (c) on FO.

7 Discussion

Although none of the loss functions fully succeed in capturing the highest–risk classes, introducing ordinality into the training process clearly improves model performance by "pushing" predictions of the most severe classes toward the intermediate class, a behavior that is not achieved when using standard cross-entropy. Among all configurations, the WKLoss achieves the best results, with a gain of more than +0.1 IoU on the extreme classes. Model calibration remains relatively similar across losses, with a persistent tendency to underestimate positive classes.

With TDeGPD, we propose a probabilistic loss designed specifically for ordinal classification.

While this loss leads to higher predicted probabilities for the extreme classes, it suffers from poor calibration, which limits the reliability of the resulting probability estimates in an ordinal classification setting.

Our results confirm the current theoretical understanding that, to achieve correct predictions on the most critical and rare classes, the model must necessarily "misclassify" some samples from lower-risk levels. This behavior arises from the inherently discrete and stochastic nature of wildfire occurrence, where many samples labeled as non-fire (zero risk) may in reality possess hidden or unobserved risk factors. Incorporating this uncertainty into both training and evaluation would therefore represent an essential step forward for advancing the state of the art.

This challenge is also evident in low-risk areas, where only a few fires are reported and precise prediction remains difficult. Incorporating seasonality and uncertainty in the occurrence of events during training appears to be a promising direction for future work. Although generating new samples through techniques such as SMOTE could seem relevant, the extremely small proportion of the highest-severity classes (e.g., only 12 class-4 samples in the test set) would introduce a substantial risk of overfitting.

8 Conclusion

In this work, we presented the first approach to ordinal classification of wildfires for the prediction of extreme events using a database directly linked to an operational application context. By comparing different ordinal loss functions with the eGPD-based method and standard cross-entropy, we demonstrated that, for the French context, the best performance is achieved using WKLoss, which provides higher accuracy while retaining similar calibration properties. However, accurate prediction of the most extreme classes remains strongly constrained by their rarity, and none of the evaluated models were able to deliver fully satisfactory results for these samples. Incorporating seasonality and explicit uncertainty regarding fire occurrence into the training process appears to be a key direction for future research.

Availability of data and material

The datasets used and analyzed during the current study are not publicly shared due to storage constraints and data ownership restrictions. However, all data can be reconstructed using the scripts and detailed instructions provided in the following open-source repository:

Localized-Forest-Fire-Risk-Prediction-ADepartment-Aware-Approach-for-Operational-DecisionSupport

Users can reproduce the dataset by (i) obtaining the raw data from the referenced public sources (e.g., BDIFF fire records, meteorological data, and satellite imagery), and (ii) executing the provided scripts following the documented workflow. The reconstruction process requires substantial storage capacity (approximately 250 GB for full national coverage).

All code of this research will be publicly available on github.

Conflict of Interest

The authors declare that they have no known competing financial interests or personal relationships that could have appeared to influence the work reported in this paper.

9 Ethical and Informed Consent

Data will be collected and used only with the participants' free, informed, and revocable consent, in full respect of their privacy and rights.

References

[1] Da Wang, Dabo Guan, Shuwei Zhu, and et al. Economic footprint of california wildfires in 2018. *Nature Sustainability*, 4(3):252–260, 2021.

[2] John M Diaz. Economic impacts of wildfire. *Southern Fire Exchange*, 498:2012–7, 2012.

[3] Matthew W. Jones, John T. Abatzoglou, Sander Veraverbeke, Niels Andela, Gitta Lasslop, Matthias Forkel, Adam J. P. Smith, Chantelle Burton, Richard A. Betts, Guido R. van der Werf, Stephen Sitch, Josep G. Canadell, Cristina Santín, Crystal Kolden, Stefan H. Doerr, and Corinne Le Quéré. Global and regional trends and drivers of fire under climate change. *Reviews of Geophysics*, 60(3):e2020RG000726, 2022.

[4] Tobias Osswald, Carla Gama, Ana Patrícia Fernandes, Diogo Lopes, Vassiliki Varela, and Ana Isabel Miranda. Effects of the wildfires in august 2021 on the air quality of athens through a numerical simulation. *International Journal of Wildland Fire*, 32:1633–1645, 2023.

[5] Suzanne E Finlay, Andrew Moffat, Rob Gazzard, David Baker, and Virginia Murray. Health impacts of wildfires. *PLoS Currents*, 4:e4f959951cce2c, Nov 2012.

[6] Hongyu Chen, Jonathan M Samet, Philip A Bromberg, and Haiyan Tong. Cardiovascular health impacts of wildfire smoke exposure. *Particle and Fibre Toxicology*, 18(1):2, Jan 2021.

[7] Wayne E. Cascio. Wildland fire smoke and human health. *Science of the Total Environment*, 624:586–595, May 2018.

[8] Emily Grant and Jennifer D. Runkle. Long-term health effects of wildfire exposure: A scoping review. *The Journal of Climate Change and Health*, 6:100110, 2022.

[9] N. Fann, B. Alman, R.A. Broome, G.G. Morgan, F.H. Johnston, G. Pouliot, and A.G. Rappold. The health impacts and economic value of wildland fire episodes in the u.s.: 2008–2012. *The Science of the total environment*, 653:427–438, 2019.

[10] Yan Boulanger, Dominique Arseneault, Annie Claude Bélisle, Yves Bergeron, Jonathan Boucher, Yan Boucher, Victor Danneyrolles, Sandy Erni, Philippe Gachon, Martin P. Girardin, Eliane Grant, Pierre Grondin, Jean-Pierre Jetté, Guillemette Labadie, Mathieu

Leblond, Alain Leduc, Jesus Pascual Puigdevall, Martin-Hugues St-Laurent, Junior A. Tremblay, and Kaysandra Waldron. The 2023 wildfire season in québec: an overview of extreme conditions, impacts, lessons learned, and considerations for the future. *Canadian Journal of Forest Research*, 55:1–21, 2025.

[11] G. Certini. Effects of fire on properties of forest soils: a review. *Oecologia*, 143(1):1–10, 2005.

[12] J. Elly, S. H. Doerr, J. Ekroos, T. S. Ibáñez, Md. R. Islam, C. Santín, M. Soares, and N. Kljun. Impacts of fire severity and salvage-logging on soil carbon fluxes in a boreal forest. *EGUsphere [preprint]*, 2024.

[13] Garros Gong, Stanko Dimitrov, and Michael R. Bartolacci. Digital strategies in wildfire management: Social media analytics and web 3.0 integration. *Discover Sustainability*, 5(1):92, 2024.

[14] Cuc Duong, Vethavikashini Chithrra Raghuram, Amos Lee, Rui Mao, Gianmarco Mengaldo, and Erik Cambria. Neurosymbolic ai for mining public opinions about wildfires. *Cognitive Computation*, 16(4):1531–1553, 2024.

[15] Spyros Kondylatos, Ioannis Prapas, Michele Ronco, Ioannis Papoutsis, Gustau Camps-Valls, Maria Piles, Miguel-Angel Fernandez-Torres, and Nuno Carvalhais. Wildfire danger prediction and understanding with deep learning. *Geophysical Research Letters*, 49(17):e2022GL099368, 2022. e2022GL099368 2022GL099368.

[16] Spyros Kondylatos, Ioannis Prapas, Gustau Camps-Valls, and Ioannis Papoutsis. Mesogeos: A multi-purpose dataset for data-driven wildfire modeling in the mediterranean, 2023.

[17] Remi Lam, Alvaro Sanchez-Gonzalez, Matthew Willson, Peter Wirnsberger, Meire Fortunato, Ferran Alet, Suman Ravuri, Timo Ewalds, Zach Eaton-Rosen, Weihua Hu, Alexander Merose, Stephan Hoyer, George Holland, Oriol Vinyals, Jacklynn Stott, Alexander Pritzel, Shakir Mohamed, and Peter Battaglia. Graphcast: Learning skillful medium-range global weather forecasting, 2023.

[18] J. Koh. Gradient boosting with extreme-value theory for wildfire prediction. *Extremes (Boston)*, 26(2):273–299, Jan 21 2023. Epub ahead of print.

[19] Daniela Cisneros, Jordan Richards, Ashok Dahal, Luigi Lombardo, and Raphaël Huser. Deep graphical regression for jointly moderate and extreme australian wildfires. *Spatial Statistics*, 59:100811, 2024.

[20] Nicolas Caron, Christophe Guyeux, Hassan Noura, and Benjamin Aynes. Localized forest fire risk prediction: A department-aware approach for operational decision support, 2025.

[21] Dimitrios Michail, Charalampos Davalas, Lefki-Ioanna Panagiotou, Ioannis Prapas, Spyros Kondylatos, Nikolaos Ioannis Bountos, and Ioannis Papoutsis. Firecastnet: Earth-as-a-graph for seasonal fire prediction, 2025.

[22] Francisco Bérchez-Moreno, Víctor M. Vargas, Rafael Ayllón-Gavilán, David Guijo-Rubio, César Hervás-Martínez, Juan C. Fernández, and Pedro A. Gutiérrez. dlordinal: a python package for deep ordinal classification, 2025.

[23] Lucas Fidon, Sébastien Ourselin, and Tom Vercauteren. *Generalized Wasserstein Dice Score, Distributionally Robust Deep Learning, and Ranger for Brain Tumor Segmentation: BraTS 2020 Challenge*, page 200–214. Springer International Publishing, 2021.

[24] Wilson Silva, João Ribeiro Pinto, and Jaime S. Cardoso. A uniform performance index for ordinal classification with imbalanced classes. In *2018 International Joint Conference on Neural Networks (IJCNN)*, pages 1–8, 2018.